QUANTIFYING GROUNDWATER DISCHARGE FROM THE VALLEY-FILL AQUIFER IN MOAB-SPANISH VALLEY NEAR MOAB, UTAH

by

Nora Claire Nelson

A thesis submitted to the faculty of
The University of Utah
in partial fulfillment of the requirements for the degree of

Master of Science

in

Geology

Department of Geology and Geophysics

The University of Utah

December 2017

The University of Utah Graduate School

STATEMENT OF THESIS APPROVAL

The thesis of **Nora Claire Nelson**

has been approved by the following supervisory committee members:

D. Kip Solomon	, Chair	**9/19/2017** Date Approved
Victor Heilweil	, Member	**9/19/2017** Date Approved
John M. Bartley	, Member	**9/20/2017** Date Approved

and by **Thure Cerling**, Chair/Dean of

the Department/College/School of **Geology and Geophysics**

and by David B. Kieda, Dean of The Graduate School.

ABSTRACT

Moab City and Grand County rely on groundwater for public water supply. Recent development and an increase in water right applications prompted area water managers to call for an updated evaluation of local groundwater resources. The purpose of this study is to (1) prepare a conceptual groundwater flow model for lower Moab-Spanish Valley by delineating flow paths and identifying sources of recharge to the valley-fill aquifer, in order to (2) quantify groundwater outflow to the Colorado River to improve estimates of groundwater available for public use. Samples were collected from 30 wells to analyze major ions, tritium, noble gases, CFCs, SF_6, and deuterium and oxygen-18 stable isotopes. The groundwater budget was evaluated by estimating discharge to the Colorado River and loss to Mill Creek. Groundwater discharge was estimated first by performing a Darcy Flux calculation. Twelve new observation wells were drilled and installed in a transect across the Scott M. Matheson Wetlands Preserve, ranging in depth from 25 to 60 feet below ground surface. Eight single-well tests and two dual-well tests were performed to determine transmissivity, which ranged from 90 to 5,400 ft^2/day, with a median of approximately 1000 ft^2/day. The hydraulic gradient was determined by creating a potentiometric surface map using water levels from both new observation wells and previously existing private wells. Discharge was estimated to be 300 acre-feet per year. A second, independent estimate of groundwater discharge was made using environmental tracer data to determine change in age across some distance along a flow path. $^3H/^3He$ ages in the valley-fill aquifer range from 0 to 57 years. Average discharge had a value of 1,000 acre-feet per year. A bromide tracer test was performed to evaluate whether some groundwater was lost to Mill Creek before discharging into the Colorado River. Gain in Mill Creek was found to be negligible. Geochemical properties of

valley wells indicate that the valley-fill aquifer is not recharged by water from Glen Canyon Group Aquifer (GCGA), as previously hypothesized by Sumsion (1971); rather, it is more likely recharged by loss from Mill and Pack Creeks.

TABLE OF CONTENTS

LIST OF FIGURES

Figure

LIST OF TABLES

Table

1 INTRODUCTION

1.1 Background

The city of Moab is cradled in the northwest end of Moab-Spanish Valley[1], near the Colorado River, in Grand County. Moab-Spanish Valley extends southeast from Moab into San Juan County, toward the headwaters of Mill Creek in the prominent La Sal Mountains.

In 2011, the San Juan Spanish Valley Special Service District (SJSVSSD), which services an unincorporated area in San Juan County, applied to permanently transfer a 5,000 acre-foot per year appropriation for surface water from the San Juan River to wells in Spanish Valley. The proposed transfer was met with opposition from private citizens and local water managers who feared additional groundwater withdrawals could negatively impact existing water rights. In 2013, the Utah Division of Water Rights granted a provisional 600 acre-feet per year out of the 5,000 requested. A decision about the remainder is pending. In 2015, a comprehensive groundwater resource study was designed to help inform this and future water management decisions. The study is jointly funded by the city of Moab, Grand County, San Juan County, the Grand County Water and Sewer Service (GCWSS), the Utah Division of Water Rights (U6i), the Bureau of Land Management (BLM), and the U.S. Forest Service (USFS).

The Moab Regional Groundwater Study is led in partnership by the USGS and the University of Utah. The USGS investigated aspects of both recharge and discharge to improve understanding of the aquifer system and its boundaries, and to update and refine the overall groundwater budget for Moab-Spanish Valley and the surrounding area. The USGS study area

[1] Moab-Spanish Valley refers to the contiguous topographic feature that, for the purposes of this report, combines the formally distinct political regions, Moab Valley and Spanish Valley, which are separated only by the county line and are located in Grand County and San Juan County, respectively.

primarily included the Mill Creek and Pack Creek drainage basins, consisting of Moab-Spanish Valley, the western slopes of the La Sal Mountains, and the slickrock mesas in-between; it extended as far north as Ice Box Canyon and included a small area of Kane Springs Creek to the south (Figure 1).

1.2 Purpose and Scope

The purpose of this study is to (1) prepare a conceptual groundwater flow model for lower Moab-Spanish Valley by delineating flow paths and identifying sources of recharge to the valley-fill aquifer, in order to (2) quantify groundwater outflow to the Colorado River to improve estimates of groundwater available for public use.

Sumsion (1971) estimated that approximately 8,000 acre-feet of groundwater per year flowed to the Colorado River through the subsurface (not including 3,000 acre-feet consumed by phreatophytes), and concluded that the primary source of recharge to the valley-fill aquifer was premodern Glen Canyon Group Aquifer (GCGA) water from springs and groundwater from the northeast. Gardner (2004), however, found that shallow groundwater near the discharge zone at the Colorado River did not resemble the geochemical signature of GCGA water — the implication being that "unless there is a considerable amount of GCG water discharging from an unknown location, […] the total flow from the GCG aquifer has been significantly overestimated." Gardner (2004) used a Darcy Flux calculation along the length of the valley adjacent to the Colorado River to estimate between 100 and 1,500 acre-ft per year of groundwater discharge to the Colorado River. This study sought to follow up on the findings of that study by collecting additional data to further investigate the groundwater in lower Moab-Spanish Valley, by attempting to locate unaccounted-for GCGA water in order to refine and/or validate the estimate of groundwater discharge to the Colorado River.

A conceptual groundwater flow model was developed for lower Moab-Spanish Valley based on geology, physical aquifer properties, and geochemical characteristics. Groundwater

samples were collected from 30 wells in lower Moab-Spanish Valley, including 10 new observation wells installed during this study within the Scott M. Matheson Wetlands Preserve (hereafter, the wetland). Samples were analyzed for major ions, dissolved noble gases, tritium, sulfur hexafluoride, chlorofluorocarbons, and stable water isotopes (^{18}O and ^{2}H). Geochemical analyses were used to categorize the samples according to groundwater type, age (time since recharge), recharge elevation, and recharge temperature.

With the conceptual model in mind, two independent methods were used to estimate groundwater discharge to the Colorado River. One method used physical aquifer properties to estimate discharge (the Darcy flux method) and the other used geochemical properties (the age gradient method).

Lastly, a bromide tracer test was performed on the lower reaches Mill Creek to locate and quantify any groundwater discharging to Mill Creek above the Colorado River.

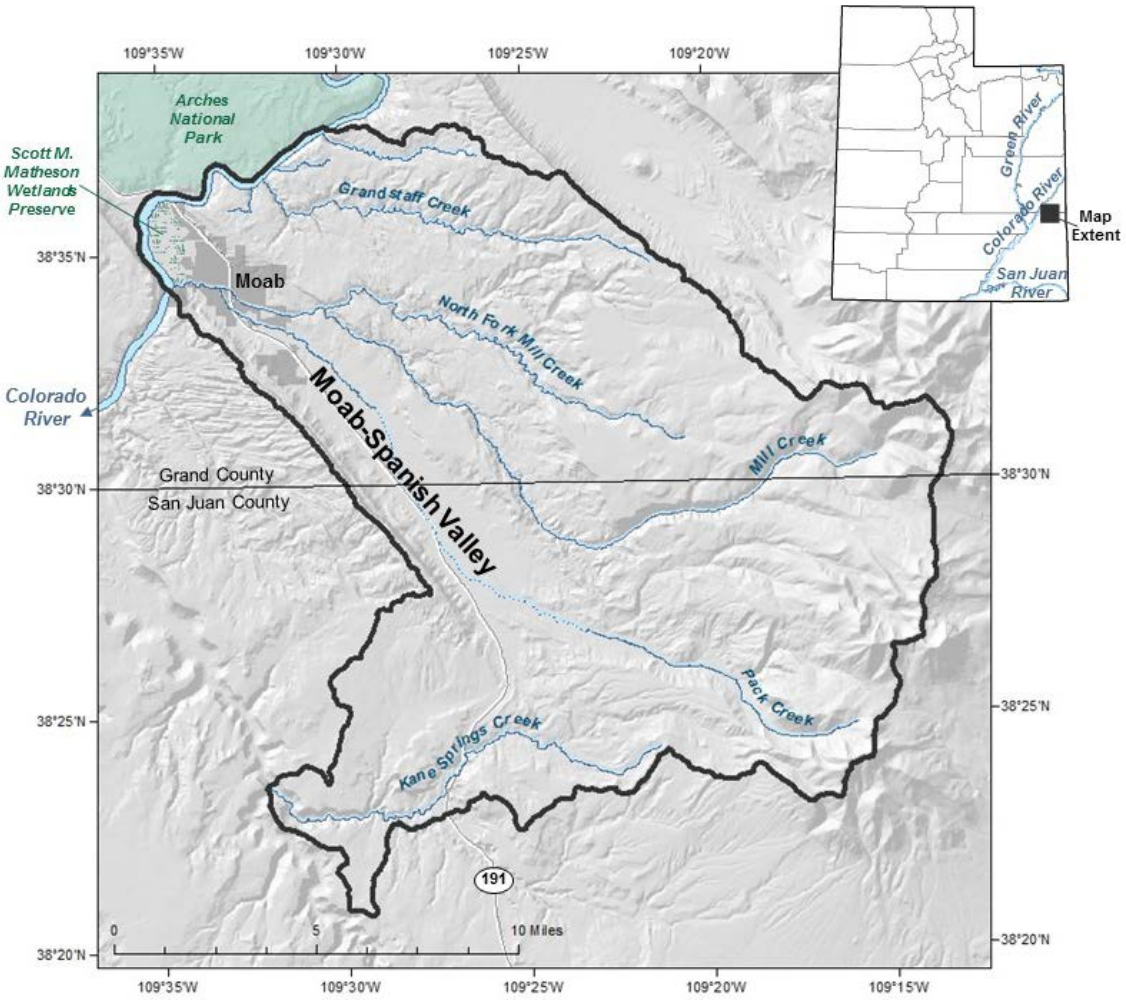

Figure 1. Map of the study area in southeastern Utah, including the city of Moab, Moab-Spanish Valley, the Scott M. Matheson Wetlands Preserve, and the Colorado River. These features comprise the study area (outlined in black), which extends southeast from Moab toward the headwaters of Pack Creek and Mill Creek in the La Sal Mountains.

2 SETTING

2.1 Geology

Moab-Spanish Valley is located in the Colorado Plateau physiographic province. It is a northwest-southeast trending topographic feature formed by the collapse of a salt anticline — one of many in the region. The Middle Pennsylvanian Paradox Formation contains sequences of evaporite salts (halite and gypsum), dolomite, and shale, which were deposited in the Paradox Basin, in the shadow of the Uncompahgre Plateau. The buoyant salts migrated into elongated diapirs, under pressure created by deposition of overlying sediments, resulting in both depositionally and tectonically formed anticlines (Doelling, 1983). Groundwater dissolution of the salts resulted in collapse of the anticlines. Paradox Formation caprock contains the leftover anhydrite (dehydrated gypsum) and shale beds after evaporites were leached away; it is exposed in the lower valley along the north and south walls of the canyon, just outside of the wetland (Figure 2).

Steep, sandstone walls rim the valley, looming nearly 800 feet above the valley floor. The oldest exposed sandstone in the lower valley is the Triassic Chinle Formation. Overlying the Chinle is the cliff-forming Jurassic Glen Canyon Group, composed of the Wingate, Kayenta, and Navajo Sandstones, in ascending order. The Moab Fault cuts through the center of the valley, downdropping the northeastern block relative to the southwest, though displacement is more pronounced in the valley north of the Colorado River.

The prominent La Sal Mountains are igneous in origin. They were intruded in the Paleogene in the form of laccoliths (Doelling et al., 2002), and were subsequently exposed by erosion of overlying sediments.

Moab-Spanish Valley is blanketed with Quaternary alluvial sediments deposited by Mill

Creek and Pack Creek as well as colluvial sediments from the valley walls. In general, finer-grained sediment is deposited toward the lower end of the valley, but paleo-stream channels of Mill Creek and the Colorado River have introduced lenses of coarse gravel.

2.2 Hydrogeology

In general, groundwater in Moab-Spanish Valley recharges at high altitudes in the La Sal Mountains, where the tallest peak is just over 12,700 feet above sea level, and discharges into the Colorado River at around 3,950 feet.

Moab-Spanish Valley has two major streams, Mill Creek and Pack Creek. Pack Creek joins Mill Creek in downtown Moab before flowing into the Colorado River (Figure 1). There are two aquifers in the study area, the Glen Canyon Group Aquifer (GCGA) and the valley-fill aquifer. The public water supply for Moab City and Grand County is sourced from springs emanating from, and wells completed in, the GCGA. Many irrigation wells produce water from the valley-fill aquifer, which is not a suitable source of culinary water.

The GCGA is located in the Glen Canyon Group sandstone formations: the Navajo, the Kayenta, and the Wingate. Although each of these formations contains at its base a lower-permeability confining bed, fracturing in the northern valley wall along the Moab Fault is sufficient to consider the formations to be hydraulically connected and thus to form one aquifer (Fillmore, 2010). The GCGA is known to contain high-quality water suitable for public water supply and is an EPA-designated sole source aquifer. The GCGA is likely recharged by high-elevation precipitation in the La Sal Mountains (Gardner, 2004). The valley-fill aquifer is known to have higher total dissolved solids (TDS) relative to the GCGA, as well as nitrate contamination.

A deep brine layer under the wetland is thought to have evolved from groundwater dissolving Paradox Formation salts (Gardner, 2004). The dimensions and extent of the brine are unknown, except where it has been encountered at shallow depths in the wetland. The density

gradient between the brine and the overlying fresh groundwater creates a barrier to flow and effectively delineates the bottom of the freshwater aquifer in the wetland.

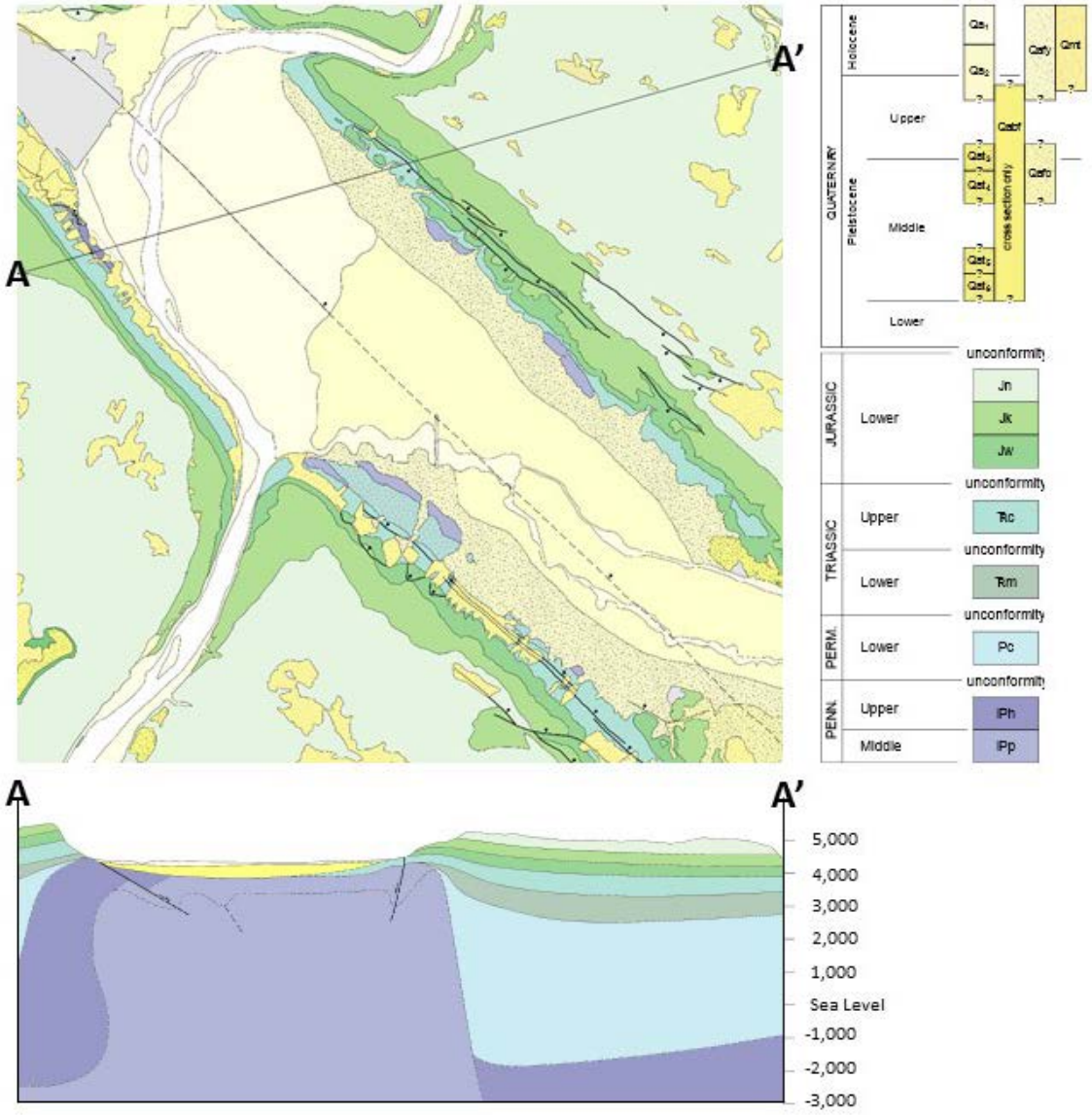

Figure 2. Geology of the study area (modified from Doelling et al., 2002). Moab-Spanish Valley is a northwest-southeast trending topographic feature formed by the collapse of a salt-anticline, related to evaporate salt deposits in the Middle Pennsylvanian Paradox Formation. The geology exposed in the lower valley includes the Triassic Chinle Formation and the Jurassic Glen Canyon Group (Wingate, Kayenta, and Navajo sandstones). The Moab Fault cuts through the center of the valley, downdropping the northeastern block relative to the southwest. Moab-Spanish Valley is blanketed with Quaternary alluvial sediments deposited by Mill Creek and Pack Creek as well as colluvial sediments from the valley walls. The public water supply for the city of Moab comes from the Glen Canyon Group Aquifer, while the valley fill sediment aquifer is used for agricultural watering.

3 METHODS

3.1 Drilling and Well Installation

Twelve wells were drilled and installed in the wetland, including eight single-completion and two dual-completion wells (Figure 3). The wells were used for aquifer testing, geochemical sampling, and hydraulic head measurements.

Well siting was guided in part by preliminary results from an electrical resistivity survey performed during this study along the Colorado River in the wetland (Briggs, written communication, February 27, 2017). The survey was conducted to locate zones of freshwater discharge along the Colorado River. The data demonstrated, at least qualitatively, that brines are shallow in the north (i.e., the uppermost freshwater layer is thin or nonexistent), whereas a thicker lens of fresh groundwater is probably present along an approximately 1 km stretch from the Mill Creek confluence to the north, and that these are separated by a brackish transition zone in the middle (Figure 4).

A Darcy flux calculation requires the dimensions of the cross-sectional area of groundwater flow. Due to the variation in thickness of the fresh groundwater zone revealed by the electrical resistivity survey, the complication of seasonal variation observed by Gardner (2004), and the uncertainty introduced by evapotranspiration in the wetland (Pataki et al., 2005), the transect of wells marking the cross-sectional area was installed on the eastern edge of the wetland rather than along the river (wells U18 through U25, Figure 3). Unfortunately, the central area between U22 and U24 was inaccessible with the drill rig due to the muddy nature of the wetland. The locations of the two well pairs (wells U26 and U27, and wells U28 and U29) were selected to verify the location and depth of the freshwater lens at its thickest point along the Colorado River, as implied by the electrical resistivity survey.

Drilling and well installation was performed by RB&G Engineering using a single-axle auger rig. The auger bit was 4 inches in outer diameter with a 1-inch flight, resulting in boreholes that are approximately 6 inches in diameter.

Wells ranged in depth from 25 to 61 feet (Figure 5). Each well was constructed with 2.5-inch schedule 40 PVC pipe with a 5-foot screened interval above a 1-foot cap. Wells were completed with coarse-grained silica sand around the well screen, bentonite backfill, and 6 feet of cement grout with either a steel or aluminum cap.

The materials encountered while drilling were primarily sand and gravel (Figure 5). While gravel did not typically rise to the surface while drilling (it was probably pushed into the sides of the borehole), it was known to be present by shaking and rattling of the drill rig. A split-spoon sample was taken during one such occurrence, and revealed pebbles up to 2 inches in diameter. Wells were completed within high-permeability gravels wherever possible.

Wells were developed using a Waterra Inertial Pump operated by a portable actuator until the water was visibly clear prior to aquifer testing with a Grundfos submersible pump.

3.2 Aquifer Testing

Eleven aquifer tests were performed on the newly completed observation wells (nine single-well aquifer tests, including one repeat, and two dual-well aquifer tests). A Grundfos submersible pump was used to create drawdown, which was recorded every second on either a Hobo or Troll transducer (1-second data were later reduced to 1-minute data for analysis). Pumping rates were measured throughout the test using a calibrated 5-gallon bucket and stopwatch and ranged from approximately 0.3—5 gpm. Duration of pumping was approximately 3 hours, after which water levels were allowed to recover for at least 30 minutes or until they had returned to static level. (Complete drawdown data for each test are found in section A-2.)

Where possible, transmissivity was estimated using the Cooper-Jacob (1946) straight-line method for drawdown data and the Theis (1935) recovery method for recovery data. In addition,

transmissivity was estimated from specific capacity.

The Cooper-Jacob (1946) straight-line method is a graphical approach to evaluating aquifer properties from drawdown in a well or wells over time. From drawdown data, transmissivity (T) was calculated as

$$T = \frac{2.3Q}{4\pi\Delta s} \quad (1)$$

where Q is the pumping rate, and Δs is the change in drawdown corresponding to one log-cycle of time on a line fit to the late-time data on a semilog plot of time versus drawdown data.

Similarly, transmissivity was calculated from recovery data as

$$T = \frac{2.3Q}{4\pi\Delta s'} \quad (2)$$

where $\Delta s'$ is the change in recovery corresponding to one log-cycle of time on a semilog plot of t/t' versus $\Delta s'$, where t is time since pumping started, and t' is time since pumping stopped (Theis, 1935; Brown et al., 1963).

The Cooper-Jacob method is an approximation of the Theis solution, and as such, the assumptions remain that the aquifer is fully confined, of infinite extent, and uniform thickness; the well is fully penetrating; and the pumping rate is constant. The Cooper-Jacob approximation is valid for late-time data when pumping duration is sufficiently long, i.e., when $u = \frac{r^2 S}{4Tt} < 0.01$, where r is the radius of the well for single-well tests and the distance from the pumping well to the observation well or wells in multiple-well tests; S is storativity (approximately equal to specific yield (S_y) in an unconfined aquifer, assumed to be 0.3); T is transmissivity, and t is time since pumping began (Cooper and Jacob, 1946). Values of u ranged from 8E-7 to 0.008, sufficiently small (less than 0.01) to justify the use of the Cooper-Jacob method.

Several assumptions were violated — namely, the aquifer was unconfined and the wells were not fully penetrating. However, a study by Halford et al. (2006) that compared transmissivity estimates of single-well tests using Cooper-Jacob analysis to known values found that "more than 90% of the unconfined aquifer transmissivities […] were within a factor of 2 of the known values" and concluded that "interpretation of single-well tests with the Cooper-Jacob method remains more reasonable than most alternatives."

Transmissivity was estimated from specific capacity by developing an empirical equation for the area, similar to Driscoll (1986), using the following equation from Theis (1935):

$$T = \frac{Q}{4\pi s_w} W(u) = \left[\frac{W(u)}{4\pi}\right] \frac{Q}{s_w} \tag{3}$$

where Q/s_w is the specific capacity of the well (the ratio of the pumping rate to the drawdown). The $[W(u)/4\pi]$ term was developed from transmissivity data produced from the other methods, resulting in the following empirical relationship:

$$T = 10 \frac{Q}{s_w} \tag{4}$$

3.3 Water Level Inventory

Water levels were measured over a 5-day period in February 2016. Each measuring point was surveyed using a Trimble Real Time Kinematics (RTK) GPS to attain the elevation above mean sea level, to an uncertainty of, for the most part, less than 0.1 feet. Water levels were taken from the measuring point with either a chalked steel tape or an electronic water level probe.

3.4 Sample Collection and Analysis

Groundwater and surface water samples were collected in Spanish Valley and the surrounding area to characterize water types and to delineate groundwater flow paths. The sample data also provided insight into the fate of high-quality Glen Canyon Group Aquifer water and the source(s) of recharge into the Spanish Valley valley-fill aquifer.

Prior to sample collection, a minimum of three casing-volumes of water were purged from each well and field parameters were allowed to stabilize.

3.4.1 Field Parameters and Alkalinity

Field parameters, including temperature, specific conductance, pH, total dissolved gases (TDG), and dissolved oxygen (DO), were collected on a calibrated Hydrolab multiparameter water quality probe. The probe was also used to take salinity profiles at two locations in the wetland, U26 and MW-10-D, to delineate the freshwater to brine transition with depth. Readings were taken every foot; the water column and probe were allowed to equilibrate for approximately 1 minute each time the probe was moved to a new position. Alkalinity was measured in the field in mg/L as $CaCO_3$ using a Hach digital titrator.

3.4.2 Major Ions

Major-ion samples were pumped through a 0.45-micron filter capsule into 250 mL polyethylene bottles that had been triple-rinsed with formation water. Cation and anion samples were collected separately, the former being preserved with nitric acid. Surface water samples were collected directly from the source, filtered, and preserved on-site. Samples were kept refrigerated before analysis. Samples were analyzed on a Metrohm 883 Basic IC Plus ion chromatograph at the Geomicrobiology Laboratory at the University of Utah in Salt Lake City, Utah.

3.4.3 Dissolved Noble Gases

Concentrations of dissolved noble gases can be used to determine groundwater recharge temperature and elevation. Noble gases in groundwater have three significant sources: (1) exchange with the atmosphere prior to recharge, (2) radioactive isotopes, and (3) excess air (Aeschbach-Hertig et al., 2000).

The partitioning of atmospheric gases into liquid water is described by Henry's law,

$$p_i = H_i C_i \tag{5}$$

where p_i is the partial pressure of gas *i* in air, H_i is the Henry solubility constant (empirically determined for each gas, dependent on temperature and salinity), and C_i is the dissolved gas concentration at equilibrium. Recharging water in the unsaturated zone is constantly equilibrating with air until it reaches the water table and is cut off from atmospheric exchange, thus preserving the dissolved gas concentration. If noble gas concentrations in each groundwater sample can be corrected for radiogenic isotopes[2] and excess air, the solubility coefficients can be used to reconstruct the temperature at which the groundwater recharged.

Excess air describes the occurrence of dissolved gas concentrations in groundwater that exceed what is possible through solubility equilibrium alone. Excess air often contains gas ratios similar to those in the atmosphere. Its occurs as air becomes trapped in pore spaces during water table fluctuations; the entrapped bubbles may be partially or fully incorporated into the groundwater through dissolution and diffusive gas exchange (Stute and Schlosser, 2000).

Dissolved noble gas samples were collected using the copper tube method according to the procedure outlined by the University of Utah Dissolved and Noble Gas Laboratory

---

[2] Radiogenic isotopes of helium, ^{3}He and ^{4}He, are produced by ^{3}H and uranium-thorium (U-Th) decay, respectively. Helium isotopes were not used in this study to calculate recharge temperature or excess air, but they are measured for the purposes of ^{3}H/^{3}He dating, and ^{4}He accumulation is a good qualitative indication of old groundwater.

(http://www.noblegaslab.utah.edu/pdfs/cu_tube_sampling.pdf). Samples were collected in 3/8-inch diameter copper tubes cut to approximately 30 inches in length. To sample, water was pumped through a copper tube from a connection as close to the wellhead as possible. The outflow was back-pressured with a regulator valve to keep the dissolved gases in solution until the sample could be sealed with refrigeration clamps. Special care was taken to ensure that gases were not introduced to or allowed to escape from the sample during collection. Samples were collected in duplicates.

Samples were analyzed at the Dissolved and Noble Gas Laboratory at the University of Utah in Salt Lake City. Prior to analysis, the dissolved gases were extracted from the water sample. In a closed system under high vacuum, the water sample was transferred from the copper tube to a stainless-steel flask. The dissolved gases were driven into a second flask using a temperature gradient induced by heating the water sample in the first flask and chilling the second flask with liquid nitrogen. The gas sample was sealed again until it was transferred to the mass spectrometer.

The heavier gases (Ne, Ar, Kr, and Xe) were analyzed on a Stanford Research Systems RGA300 quadrupole mass spectrometer. Helium isotopes (^{3}He and ^{4}He) were analyzed on a Mass Analyzer Products 215-50 magnetic sector field mass spectrometer.

Recharge temperature and excess air were determined using the closed-system equilibration (CE) model, which "assumes equilibrium is attained in a closed system of initially air-saturated water and finite volume of entrapped air under constant hydrostatic pressure,"

$$C_i = C_i^* + \frac{(1-F)A_e z_i}{1+FA_e z_i/C_i^*} \quad (6)$$

where C_i is the gas concentration in solution, C_i^* is the moist-air solubility equilibrium concentration (a function of temperature, salinity, and total atmospheric pressure), A_e is the initial

volume ratio of trapped air to water, z_i is volume fraction of each gas in dry air, and *F* is the fractionation parameter describing the degree of excess air fractionation from no excess air to pure excess air (Aeschbach-Hertig et al., 2000).

The system of four equations, one for each of four gases (Ne, Ar, Kr, and Xe), is sufficient to solve for three parameters (A_e, recharge temperature, and *F*). (Salinity was assumed to be negligible because the source of recharge is meteoric; see section 4.3.4 on stable isotopes.) Although in concept it is possible to also solve for recharge elevation (if unknown), the system of equations would no longer be overdetermined and measurement errors would lead to a non-unique determination of elevation (Manning and Solomon, 2003).

A best fit model is determined by minimizing the sum of chi-squared (χ^2),

$$\chi^2 = \sum_i \frac{\left(C_i - C_i^{mod}\right)^2}{\sigma_i^2} \quad (7)$$

where, C_i is the measured concentration of gas *i*, C_i^{mod} is the modeled concentration, and σ_i is standard deviation in the measurements (Aeschbach-Hertig et al., 1999). The modeled concentrations are generated by perturbing the model parameters (A_e, recharge temperature, and F) within a theoretical range.

3.4.4 Tritium

Tritium (^{3}H) is a radioactive isotope of hydrogen used to date young groundwater. Tritium decays by beta emission to the noble gas ^{3}He with a half-life of 12.32 years. Small amounts of tritium are generated naturally through cosmic bombardment in the upper atmosphere, but above-ground nuclear testing in the 1950s and 1960s introduced large quantities

of tritium to the atmosphere, increasing natural background concentrations of 3—6 TU[3] (Kaufman and Libby, 1954) to concentrations in excess of 5000 TU at its peak in the 1960s (Solomon and Cook, 2000) (Figure 6).

Tritium samples were collected with no head-space in 500 mL low density polyethylene (LDPE) bottles, triple-rinsed with formation water. A duplicate sample was collected as backup.

The ^{3}H/^{3}He age is defined as

$$t_{^3H/^3He} = \lambda^{-1} ln\left(\frac{^3He_{trit}}{^3H} + 1\right) \quad (8)$$

where $t_{^3H/^3He}$ is the ^{3}H/^{3}He age, λ is the ^{3}H decay constant, and $^3He_{trit}$ is tritiogenic ^{3}He (Solomon and Cook, 2000). The ^{3}H component was measured at the Dissolved and Noble Gas Laboratory at the University of Utah using the helium ingrowth method (Clarke et al., 1976) using a Helix Split Flight Tube (SFT) sector field mass spectrometer.

The tritiogenic ^{3}He component was attained by correcting total ^{3}He ($^3He_{tot}$) (see section 3.4.3 on dissolved noble gas methods for description of helium measurement). The total amount of ^{3}He in the sample can be expressed as

$$^3He_{tot} = {}^3He_{atm} + {}^3He_{trit} + {}^3He_{nuc} + {}^3He_{man} \quad (9)$$

where $^3He_{atm}$ is helium from the atmosphere, $^3He_{trit}$ is helium produced by tritium decay used for age dating, $^3He_{nuc}$ is helium produced by nuclear reactions in the subsurface, and $^3He_{man}$ is helium from the mantle (Solomon and Cook, 2000). Mantle sources of ^{3}He were assumed to be negligible. Atmospheric helium is further subdivided into two components:

---

[3] Tritium concentrations are reported in tritium units (TU), where one TU is equal to one molecule of $^3H^1HO$ in 10^{18} molecules of ^1H_2O.

$$^3He_{atm} = {}^3He_{sol} + {}^3He_{exc} \quad (10)$$

where $^3He_{sol}$ is from solubility equilibrium with the atmosphere, and $^3He_{exc}$ is from excess air (Solomon and Cook, 2000). The following equation from Solomon and Cook (2000) was used to solve for $^3He_{trit}$:

$$^3He_{trit} = {}^4He_m R_0 - R_{sol}[{}^4He_{sol} + (Ne_m - Ne_{sol})\alpha' R_{He-Ne}] \\ -R_{rad}[{}^4He_m - {}^4He_{sol} - (Ne_m - Ne_{sol})R_{He-Ne}] \quad (11)$$

where ^4He_m is total measured ^4He, R_0 is the $^3He/^4He$ ratio in the sample at time of collection, R_{sol} is the $^3He/^4He$ expected ratio for water in equilibrium with the atmosphere at the specified recharge elevation, $^4He_{sol}$ is the expected ^4He concentration for water in equilibrium with the atmosphere at the specified recharge elevation, Ne_m is total measured neon, Ne_{sol} is the solubility neon concentration, α' is the air-water isotope fractionation factor, R_{He-Ne} is the ratio of helium to neon in the atmosphere, and R_{rad} is the ratio of $^3He_{nuc}/^4He_{rad}$.

3.4.5 Sulfur Hexafluoride

SF_6 is an industrial compound whose presence in the atmosphere can be used to date young groundwater. Industrial production of SF_6 began in 1953 for its use as an electrical insulator (Busenberg and Plummer, 2000). It was first detected in the atmosphere in 1970 at 0.03 pptv (Lovelock, 1971). The low solubility of SF_6 in water and subsequent long residence time in the atmosphere has allowed the atmospheric mixing ratio to increase steadily over time to the current (January 2017) value of 9.26 pptv (Figure 6). Its stable, non-reactive nature, even in very reducing environments (Wilson and Mackay, 1993), adds to its usefulness as a tracer. Although most SF_6 in groundwater is anthropogenic in origin, it is naturally produced in relatively small quantities in some igneous environments (Koh et al., 2007); Heilweil (2014) also found evidence

of natural production of SF_6 from crustal sources.

SF_6 samples are collected in 1-liter amber glass bottles that were safety coated on the outside with plastic, and sealed with Polyseal cone-lined caps. To collect the sample, tubing from the pump was placed at the bottom of the sample bottle, allowing water to overflow until at least three sample-volumes have been purged through the sample bottle. The bottle was then capped with no head space and sealed with electrical tape. Samples were collected in duplicate. After collection, the samples were kept in a cooler to prevent overheating, water expansion, and bottle breakage.

SF_6 samples were analyzed at the Dissolved and Noble Gas Laboratory at the University of Utah on a Shimadzu GC-8A gas chromatograph. The resulting measured concentrations were corrected for excess air, determined independently from noble gas analysis (see section 3.4.3). The partial pressure of SF_6 during air-water equilibrium at the water table prior to recharge was calculated using the following equation from Busenberg and Plummer (2000):

$$x_{SF_6} = \frac{c_{SF_6}}{K_H}\left(P - p_{H_2O}\right) \tag{12}$$

where x_{SF_6} is the dry air mole fraction of SF_6, c_{SF_6} is the concentration of SF_6 in the sample, corrected for excess air, K_H is the Henry's law constant, P is the total atmospheric pressure, and p_{H_2O} is the partial pressure of water. K_H was calculated according to Bullister et al. (2002) and is a function of salinity and recharge temperature (determined from dissolved noble gas analysis). The resulting calculated partial pressure was related back to the air mixing curve through time (Figure 6). Data prior to 1970 have been reconstructed by Maiss et al. (1994); subsequent data were taken from NOAA measurements at Niwot Ridge, Colorado.

3.4.6 Chlorofluorocarbons

CFCs are industrial compounds whose presence in the atmosphere can be used to date young groundwater. CFCs were developed in the 1930s as refrigerants. Overall production was limited in 1987, after it was discovered that CFCs were significant contributors to atmospheric ozone depletion. Production nearly ceased entirely in 1996 in accordance with the Clean Air Act. Air mixing ratios peaked in 1994, 2002, and 1995, for CFC-11, CFC-12, and CFC-113, respectively (Figure 6). CFC-11, CFC-12, and CFC-113 can be used to date groundwater back to 1947, 1941, and 1955, respectively (Plummer and Busenberg, 2000).

CFC samples were collected in 125 mL clear glass bottles, sealed with foil-lined caps. Samples were collected through refrigeration-grade copper tubing to avoid desorption of atmospheric CFCs from plastic tubing. Before collection, sample bottles and caps were triple-rinsed with formation water. To collect samples, copper tubing was inserted into the sample bottle to the bottom. Once the bottle is overflowing, it is submerged in a bucket of formation water. The bottle was allowed to overflow until at least three sample-volumes were purged through the bottle, and was capped while still underwater, without head space. Samples were collected per the procedure outlined by the USGS Reston Groundwater Dating Laboratory. Samples were collected in sets of four, and were stored at room temperature away from sunlight before analysis.

CFC samples were analyzed at the Dissolved and Noble Gas Laboratory at the University of Utah on a custom-fabricated line using a Shimadzu purge and trap system based on Bullister et al. (2002).

3.4.7 Stable Isotopes

Stable isotope ($\delta^{18}O$ and $\delta^{2}H$) compositions can be used to trace groundwater provenance because of the physical processes that govern their distribution. Stable isotope compositions are reported in δ (delta) notation,

$$\delta = \left(\frac{R}{R_{std}} - 1\right) \times 1000\ ‰ \quad (13)$$

where R is the ratio of $^{18}O/^{16}O$ or $^{2}H/^{1}H$ in the sample, R_{std} is the ratio in the standard (VSMOW, Vienna Standard Mean Ocean Water), and ‰ is the unit permil.

Isotopic compositions of meteoric waters are linearly correlated, falling along the global meteoric water line (GMWL) defined by Craig (1961) as:

$$\delta D = 8\,\delta^{18}O + 10 \quad (14)$$

Mass-dependent isotope fractionation during phase changes (i.e., evaporation, condensation) results in enrichment of the heavier isotope in the denser phase (e.g., during precipitation, the heavy isotopes, ^{18}O and ^{2}H, are preferentially rained out). Removal of the precipitated water from the cloud mass (by a process approximately described by Rayleigh distillation) results in increasingly isotopically depleted waters, which can be correlated geographically with latitude, distance from shorelines, and altitude.

Stable isotope samples were pumped through a 0.45-micron filter capsule into 60 mL polyethylene bottles that had been triple-rinsed with formation water. Stable isotope samples were analyzed in the Spatio-Temporal Isotope Analytics Laboratory (SPATIAL) on a Picarro CRDS (cavity ring-down spectroscopy) water isotope analyzer.

3.5 Bromide Tracer Test

A bromide tracer test was performed along Mill Creek near the Colorado River to evaluate whether groundwater was discharging into Mill Creek before reaching the Colorado River. The need for the tracer test was prompted by flow measurements taken with a SonTek FlowTracker Handheld-ADV (Acoustic Doppler Velocimeter) that indicated a gain of

approximately 1 cfs on a 1 mile reach of lower Mill Creek. A bromide tracer injection was designed to locate and quantify the gain. A bromide tracer injection uses a concentrated solution of sodium bromide (NaBr) injected at a constant, known rate, whereby any dilution in measured concentrations of samples taken downstream indicate the occurrence of groundwater inflow (seepage) into the stream. See a detailed description of bromide tracer test methods in section A-1.

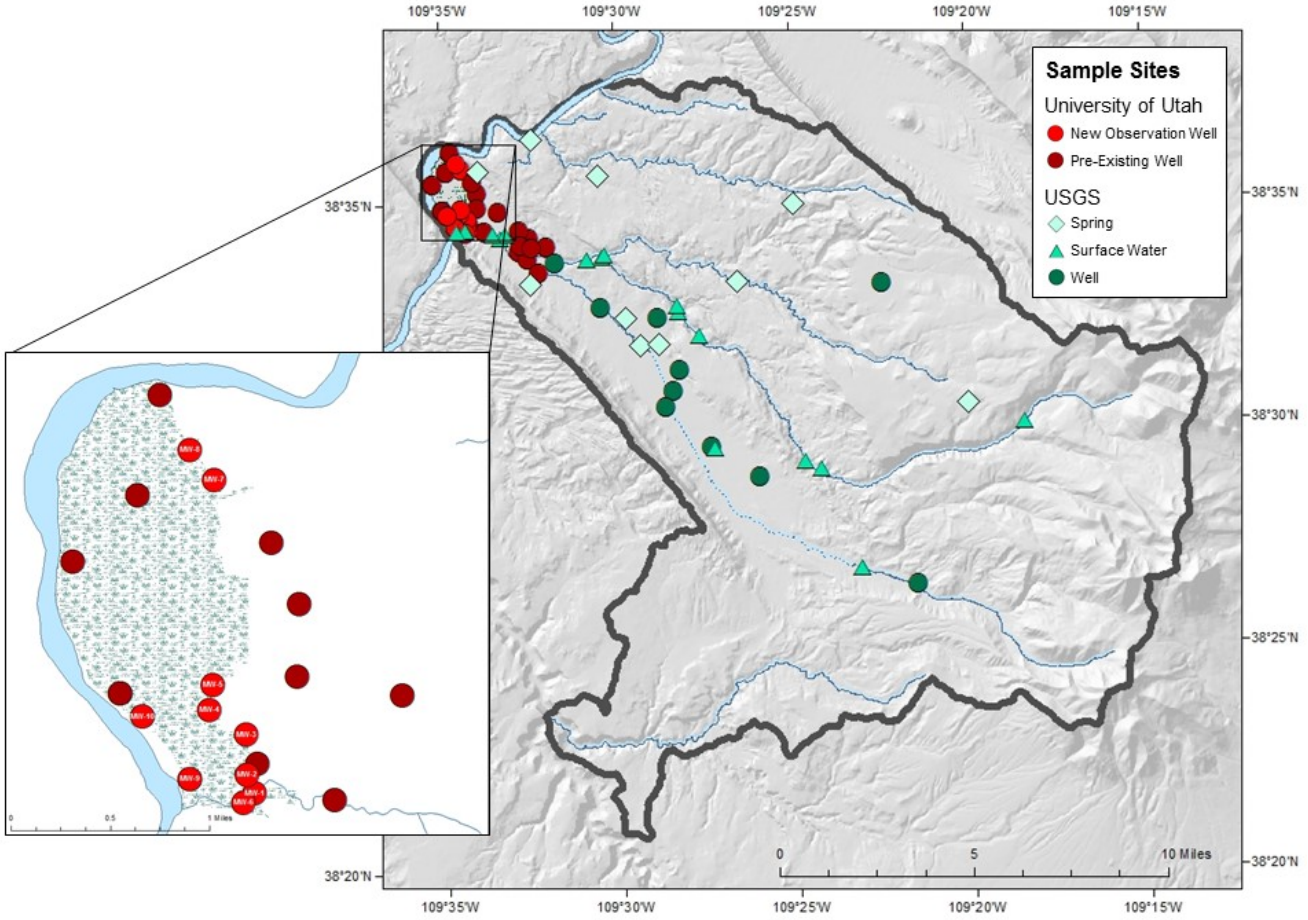

Figure 3. Map of sampling network in the study area, showing both the locations of newly installed observation wells and pre-existing wells. Wells sampled by the University of Utah in 2015-2016 are indicated in red; bright red indicates locations where wells were drilled and installed during the 2015-2016 field effort. Locations sampled by the U.S. Geological Survey (USGS) (data included in this report) are indicated in green; these locations include groundwater wells (circles), springs (diamonds), and surface water (triangles).

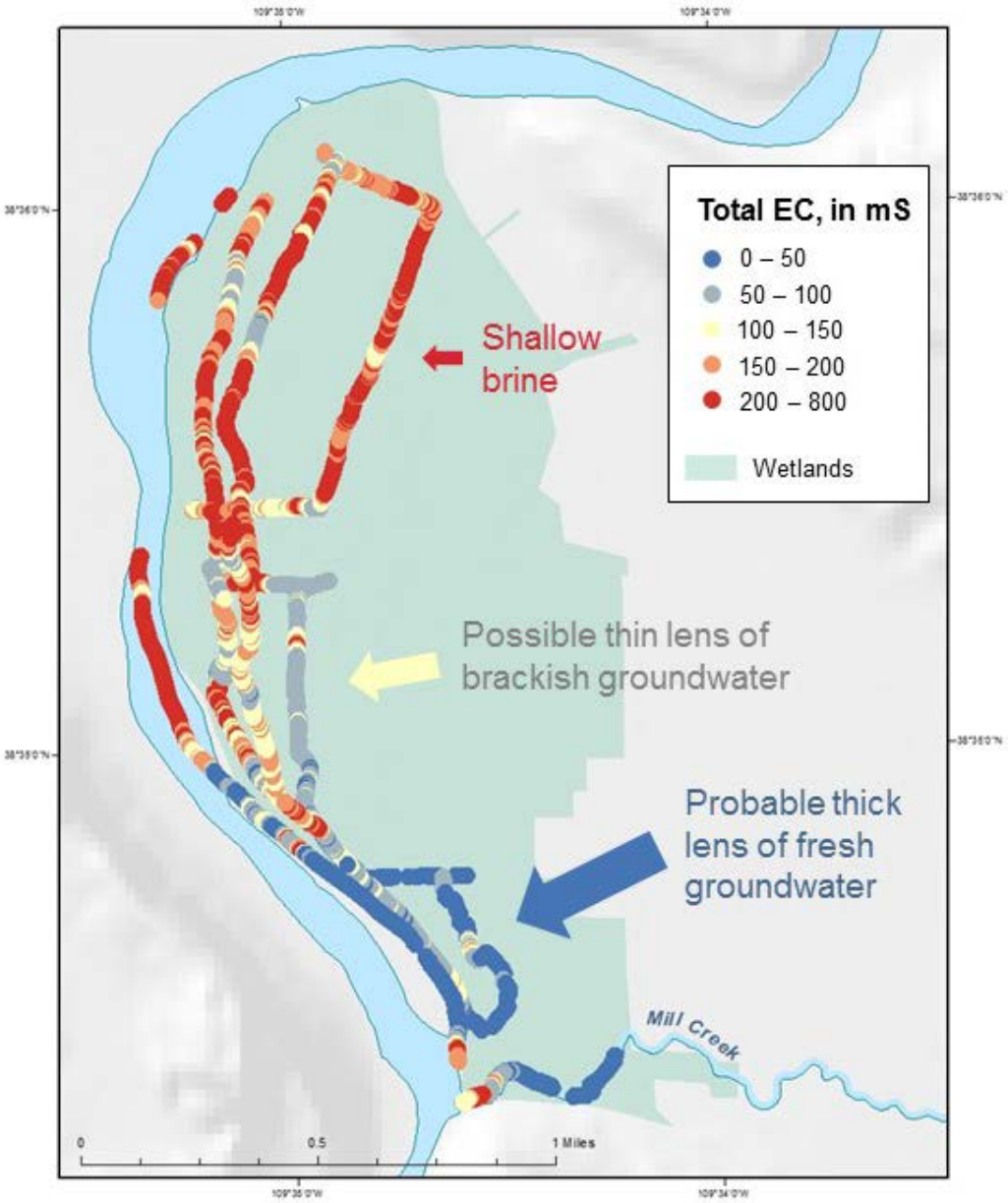

Figure 4. Preliminary results from an electrical resistivity survey (modified from Briggs, written communication, February 27, 2017) to investigate shallow alluvial groundwater discharge into the Colorado River. The map shows the total electrical conductivity (EC) in milliSiemens (mS) for shallow alluvial aquifer groundwater in the Matheson Wetlands. The data demonstrated groundwater discharge in the north is dominated by shallow brines with thin to no indication of freshwater. However, the data indicate that a thicker lens of fresh groundwater is present along the 0.5-mile reach from the Mill Creek confluence to the north. The brine and freshwater discharge areas are separated by a brackish transition zone in the middle.

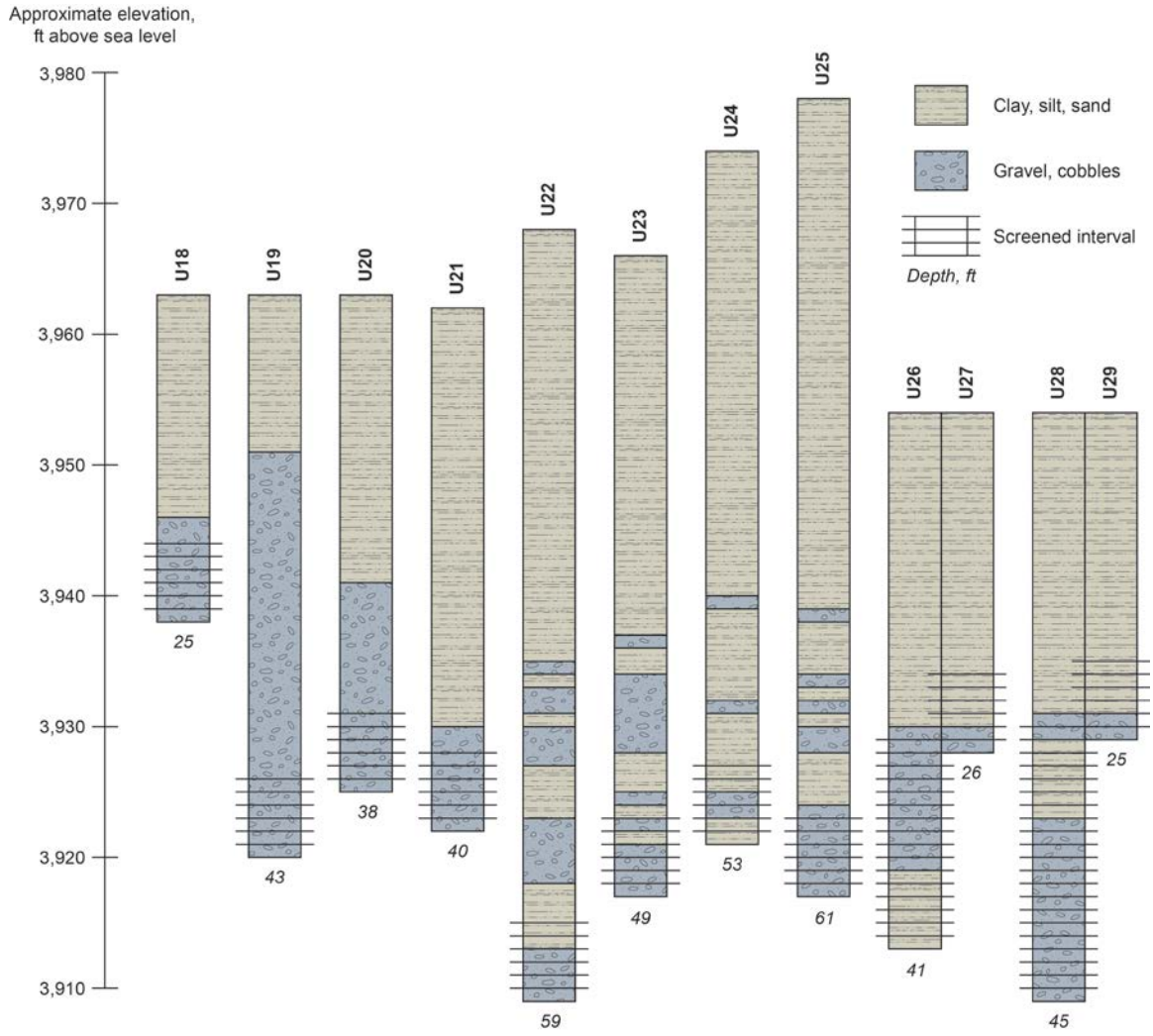

Figure 5. Lithologic logs for observation wells installed during this study, showing simplified lithology, depth, and well screen interval. The 12 observation wells include 8 single-completion wells (U18 through U25) and two dual-completion wells (U26, U27; and U28, U29). The lithologic logs are aligned from approximately north to south (see Figure 3 for locations).

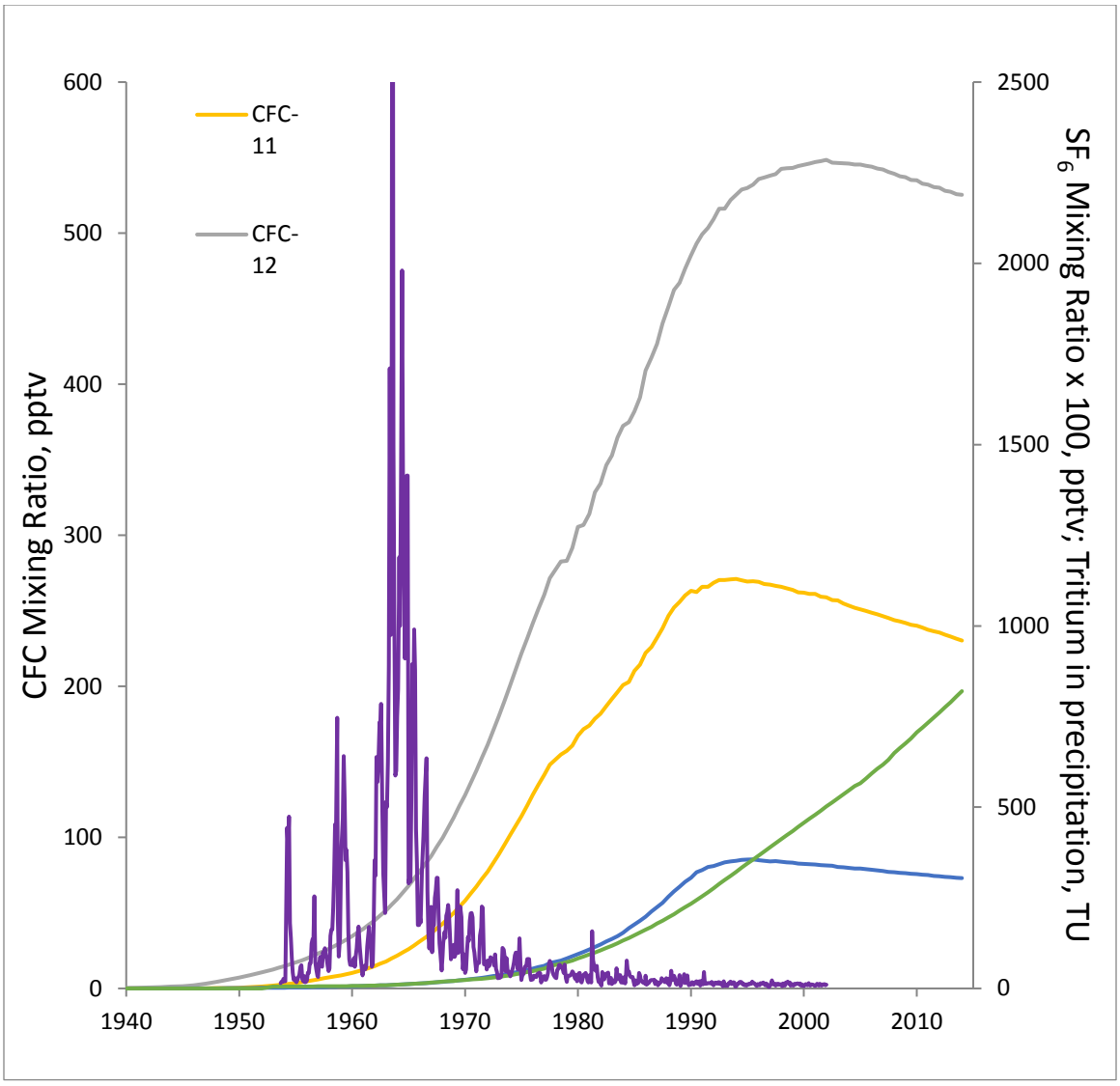

Figure 6. Reference diagram showing air-mixing curves for SF_6 (in pptv x 100); CFC-11, CFC-12, and CFC-113 (in pptv); and tritium in precipitation (in tritium units, TU) (USGS Groundwater Dating Laboratory).

4 RESULTS

4.1 Aquifer Properties

4.1.1 Transmissivity

Transmissivity estimated using the Cooper-Jacob straight-line method for drawdown data ranged from 60 to 4,100 ft^2/day (Table 1). In several cases, drawdown affected the pumping rate in such a way that the water level experienced an initial dramatic drop and then rose steadily for the remainder of the test (see U23 and U24 drawdown curves, section A-2); as a result, in these cases, transmissivity could not be estimated from Cooper-Jacob analysis of the drawdown data. Transmissivity estimated from specific capacity ranged from 80 to 6,200 ft^2/day. Transmissivity estimated using the Theis recovery method ranged from 60 to 5,900 ft^2/day. The recovery data had too much noise in the case of U18, and the test was terminated prematurely in the case of U23. Therefore, transmissivity could not be estimated in these cases.

Overall, average transmissivities at each aquifer test site using all available methods ranged from 90 to 5,400 ft^2/day, with a median of approximately 1000 ft^2/day (Figure 7). Standard deviation at each test site ranged from 0 to 920 ft^2/day.

4.1.2 Potentiometric Surface (Water Table)

Hydraulic head values derived from water-level measurements were contoured to evaluate general directions of groundwater flow (Figure 8). Head values range from 4,000 to 3,950 in the lower end of the valley. There is a notable flattening of the hydraulic gradient (from 0.02 to 0.005) to the west / northwest of the 3,990 ft contour. This could signify a change in transmissivity, either because of an increase in aquifer thickness or an increase in hydraulic conductivity. The hydraulic head contours abut the north valley wall at an angle less than 90

degrees, implying that some amount of groundwater is moving from the GCGA to the valley-fill aquifer along the north wall of the valley near the wetland.

4.2 Hydrochemistry

4.2.1 Field Parameters

Field parameters and alkalinity data are summarized in Table 2. The lowest measured specific conductivity was 680 µS/cm, and two samples exceeded the meter's detection limit of 100,000 µS/cm. The data from specific conductivity profiles at two locations (U26 and U28) are presented in Table 3; the data show the transition to brine occurring at approximately 30 feet below the measuring point in both wells (Figure 9).

4.2.2 Major Ions and Alkalinity

Major ion concentrations are summarized in Table 4. Charge balances ranged from 0 to 23%. For freshwater samples, charge balances were within 10%. Samples with poor charge balances (greater than 10%) were either from brine or brine-affected water. (The brines are high in ammonia, and the elution time between chloride and ammonia is small, making it difficult to separate the peaks.) Total dissolved solids (TDS) ranged from 533 to 159,201 mg/L. Stiff diagrams of the major-ion chemistry (Figure 10) demonstrate that water types generally fall into three categories: (1) low-TDS calcium-bicarbonate, (2) moderate-TDS calcium-sulfate, and (3) high-TDS sodium-chloride. Alkalinity ranges from 124 to 314 mg/L as $CaCO_3$.

High-quality low-TDS calcium-bicarbonate waters are characteristic of the Glen Canyon Group Aquifer (Steiger and Susong, 1997; Gardner, 2004). This geochemical signature is exhibited by wells located on the Glen Canyon Group slickrock plateau between Spanish Valley and the La Sal Mountains, groundwater emanating from springs on the north wall of Spanish Valley where it abuts the plateau, and surface water in Mill Creek prior to entering Spanish Valley. Moderate-TDS calcium-sulfate type waters are ubiquitous in the valley-fill aquifer, and

are also found in Pack Creek before it enters the valley. The high-TDS sodium-chloride brines are located at the distal end of the valley, near the Colorado River, and are attributed to dissolution of Paradox Formation salts.

4.3 Environmental Tracers

4.3.1 Dissolved Noble Gases

Measured dissolved noble gas concentrations are presented in Table 5. Values of R/R_a ranged from 0.067 to 2.053. Calculated recharge temperature (T_{rech}) and excess air (A_e) results calculated using the closed-system equilibration (CE) model assuming a recharge elevation of 1500 m are presented in Table 6. Recharge temperatures ranged from 8 to 19ºC (with one outlier of 30 ºC removed), and excess air ranged from 4.3E-4 to 0.15. Most samples showed good fits to the CE model; the average sum of chi squared was 0.5. The recharge temperature and excess air parameters were used in the analyses of $^3H/^3He$, SF_6, and CFC apparent ages.

4.3.2 Tritium

Measured and calculated parameters associated with $^3H/^3He$ age dating are presented in Table 7. Measured tritium values ranged from 0.01 to 4.79 TU. Calculated $^4He_{terr}$ ranged from -3.47×10^{-9} to 9.37×10^{-6}. Calculated $^3He_{trit}$ ranged from -3.35 to 163 TU, resulting in $^3H/^3He$ ages that ranged from 0[§] to 164 years. In general, the $^3H/^3He$ ages increase down-gradient (Figure 11).

The uncertainty associated with $^3H/^3He$ ages ranges from 0 to 154 years, with many values falling between 0 and 8 years. The uncertainty is calculated by perturbing the parameters in equation 11 within their respective ranges of error. Groundwater ages of old waters are less sensitive to error in the $^3He_{trit}$ component, because the proportion of $^3He_{trit}$ to total measured ^3He

[§] Negative $^3H/^3He$ ages from negative $^3He_{trit}$ were reported with an age of 0 years.

increases in any given sample over time as more ^{3}H decays to tritiogenic ^{3}He. However, the $^{3}H/^{3}He$ age uncertainty can also increase with large values of excess air and terrigenic ^{4}He; the fraction of total He that comes from $^{3}He_{trit}$ decreases with increasing $^{3}He_{Ae}$ (from excess air) and $^{3}He_{rad}$ (from $^{4}He_{terr}$), increasing the uncertainty in $^{3}He_{trit}$, and with it, the apparent age (Solomon and Cook, 2000).

For mixtures of young and old (i.e., tritiated and nontritiated) waters, the $^{3}H/^{3}He$ age is biased toward the young fraction (Solomon and Cook, 2000). Several samples were flagged as possible mixtures of young and old water. For example, the U11 sample had a calculated age of 0 years, which is consistent with a measured tritium of 3.14 TU (Table 7), but it has a low R/Ra value, which is a first-order indicator of the presence of older water. An R/Ra of less than 1 is likely due to the presence of terrigenic helium-4, which builds up over time in old waters due to radiogenic decay of U and Th (Solomon and Cook, 2000).

In addition to analytical error, there are uncertainties due to sampling: ages vary due to the depth of the well, and the screened interval of the well, and the permeability of the sediments over the screened interval. Ideally, $^{3}H/^{3}He$ ages would represent a flow-weighted average over the entire thickness of the aquifer.

Despite the uncertainty outlined above, $^{3}H/^{3}He$ age-dating is generally considered to be the most robust of the groundwater age-dating methods used in this study because the ^{3}H atom is physically incorporated in the water molecule and is, therefore, a conservative tracer, unlike SF_6 and CFCs, which are subject to contamination and degradation in some chemical environments.

4.3.3 Sulfur Hexafluoride

Measured SF_6 concentrations range from 0 to 11 fMol/kg (Table 8). Calculated mixing ratios range from 0 to 31 pptv. The current atmospheric mixing ratio of SF_6 is 9.26 pptv (January 2017). Samples with no measurable SF_6 presumably recharged before significant concentrations of SF_6 were introduced to the atmosphere and are considered “premodern.” Apparent ages range

from 0 to premodern, and correspond to recharge years from 2017 to pre-1953. Samples are considered "contaminated" if the calculated mixing ratio is greater than what is possible simply due to air-water equilibrium exchange during recharge (in other words, if the calculated mixing ratio is greater than the current atmospheric mixing ratio). Ten of the 30 samples are contaminated, up to three times the current (January 2017) atmospheric mixing ratio.

Samples were initially analyzed for SF_6 for comparison to $^3H/^3He$ ages; however, extensive contamination of lower Moab-Spanish Valley samples precludes this. Ten samples had calculated mixing ratios above the theoretical maximum for mere air-water equilibration at the water table prior to recharge. Additional samples, for which an SF_6 apparent age was theoretically calculable, generally skew younger than the corresponding $^3H/^3He$ apparent ages (Figure 12), suggesting these are also affected by an additional source of SF_6, whether natural or anthropogenic.

Replicates were run for all but three samples, where either the bottle or cap was cracked. Measured replicate concentrations are plotted in Figure 13. Standard deviations are within 10% for the majority (18 out of 30) samples. The agreement between replicate samples suggests that SF_6 contamination is not due to error in sampling or analytical methods.

Busenberg and Plummer (2000) described total SF_6 below,

$$SF_{6\,total} = SF_{6\,eq} + SF_{6\,exc} + SF_{6\,terr} + SF_{6\,cont} - SF_{6\,loss} \quad (15)$$

where $SF_{6\,eq}$ is due to equilibrium air-water exchange, $SF_{6\,exc}$ is addition from excess air during the dissolution and incorporation of air bubbles into the groundwater during water table rise, $SF_{6\,terr}$ is addition of natural SF_6, $SF_{6\,cont}$ is the addition of anthropogenic concentration, and $SF_{6\,loss}$ is any loss due to degradation. If terrigenic SF_6 and SF_6 from contamination and SF_6 loss are small, and excess air is determined independently, it is possible to date young groundwater

with SF_6.

Loss of SF_6 was assumed to be negligible (and any loss of SF_6 would make the contamination due to terrigenic or anthropogenic sources even more pronounced), so we focused on the potential sources of terrigenic or anthropogenic contamination.

There is a strong spatial element to the contamination, relating to the lower valley and the wetland. Samples indicated in orange (Figure 12) were taken from wells within the wetland boundaries, except the U10 well, which is just upgradient (Figure 3). Gross contamination is not limited to the wetland; but, in general, contamination increases toward the Colorado River, especially when considered in relationship to samples taken for the USGS partner study in the upper valley (Figure 14).

Many of the contaminated samples are from wells containing brine or brine-affected water; however, contamination does not appear to be inherently associated with the brines because the true brines (U4 and U5) contain essentially no SF_6 (Figure 15). Since the deep brines at U4 and U5 do not exhibit any SF_6, it seems unlikely that there is a natural terrigenic source, and more plausible that recent contamination is only affecting the shallower wells.

Potential anthropogenic sources include the Ferrellgas underground injection site and the Atlas Mill Tailings. The Ferrellgas site was shut down in 2003 after failing mechanical integrity testing. The source of SF_6 in the wetland remains an interesting research question, but is beyond the scope of this study.

4.3.4 Chlorofluorocarbons

Measured CFC data are summarized in Table 9; values ranged from 0.015—17.4 pMol/kg for CFC-11, 0—69.7 pMol/kg for CFC-12, and 0—0.385 pMol/kg for CFC-113. Mixing ratios were calculated based on an assumed recharge elevation of 1500 m and recharge temperatures from dissolved noble gas analysis also based on a 1500 m recharge elevation. Mixing ratios ranged from 1.1—990 pptv for CFC-11, 0—20.2 pptv for CFC-12, and 0—72.1

pptv for CFC-113 (Table 10). These mixing ratios resulted in apparent ages that ranged from premodern to 0 years for CFC-11 and CFC-12, and 32 to 74 for CFC-113 (Table 11).

Except for two samples (U7 and U15) that fall along the piston flow mixing line, CFC-11 appears to be degraded when plotted against CFC-12 (Figure 16). CFCs, especially CFC-11, are known to degrade in some anaerobic environments (Plummer and Busenberg, 2000). CFC-12 and CFC-113 concentrations are somewhat consistent along a piston flow model for samples older than approximately 35 years (Figure 16); the younger samples may have been affected by loss of CFC-113 due to sorption (Plummer and Busenberg, 2000). CFC-12 is generally considered to be the most stable CFC, and the most useful for groundwater age-dating.

4.3.5 Stable Isotopes

Stable isotope data are presented in Table 12. Isotopic compositions range from -15 to -13.5 for $\delta^{18}O$ and -108.8 to -101.5 for $\delta^{2}H$. The isotopic distribution was plotted in reference to the global meteoric water line (GMWL) and the Utah meteoric water line (UMWL) in Figure 17. All of the samples appear to be of meteoric origin, based on correlation with the GMWL. Several samples (namely, the brines) plot below the GMWL, an indication of evaporative enrichment.

GCGA water is defined by Gardner (2004) as having $\delta^{18}O$ of -14.5 to -15.0. Many of the samples appear to have been sourced from precipitation occurring at high elevation, similar to the GCGA end member.

4.4 Mill Creek Seepage (Bromide Tracer Test)

The injected bromide concentration in the stream reached steady-state after approximately 4 hours (Figure 18). During the 18-hour period of steady-state, the bromide concentration in the stream increased steadily over time; this is a result of the stream flow declining steadily over the same time period, as the test was conducted on the tail-end of a rain event, as indicated by transducer data (Figure 19).

A synoptic sampling campaign (Figure 20) showed a gain of approximately 2.7 cfs below the confluence of Mill Creek and Pack Creek (due to inflow of Pack Creek), but less than 0.1 cfs of gain between Pack Creek and the Colorado River.

The streamflow measurements that prompted the bromide tracer test indicated about 1 cfs of gain into a stream with a total flow rate of approximately 10 cfs. The measured gain is approximately 10 % of the total streamflow, which is near the error associated with manual streamflow measurements (approximately 5 %). It is, however, possible that the measured gain was real, but that it occurs intermittently.

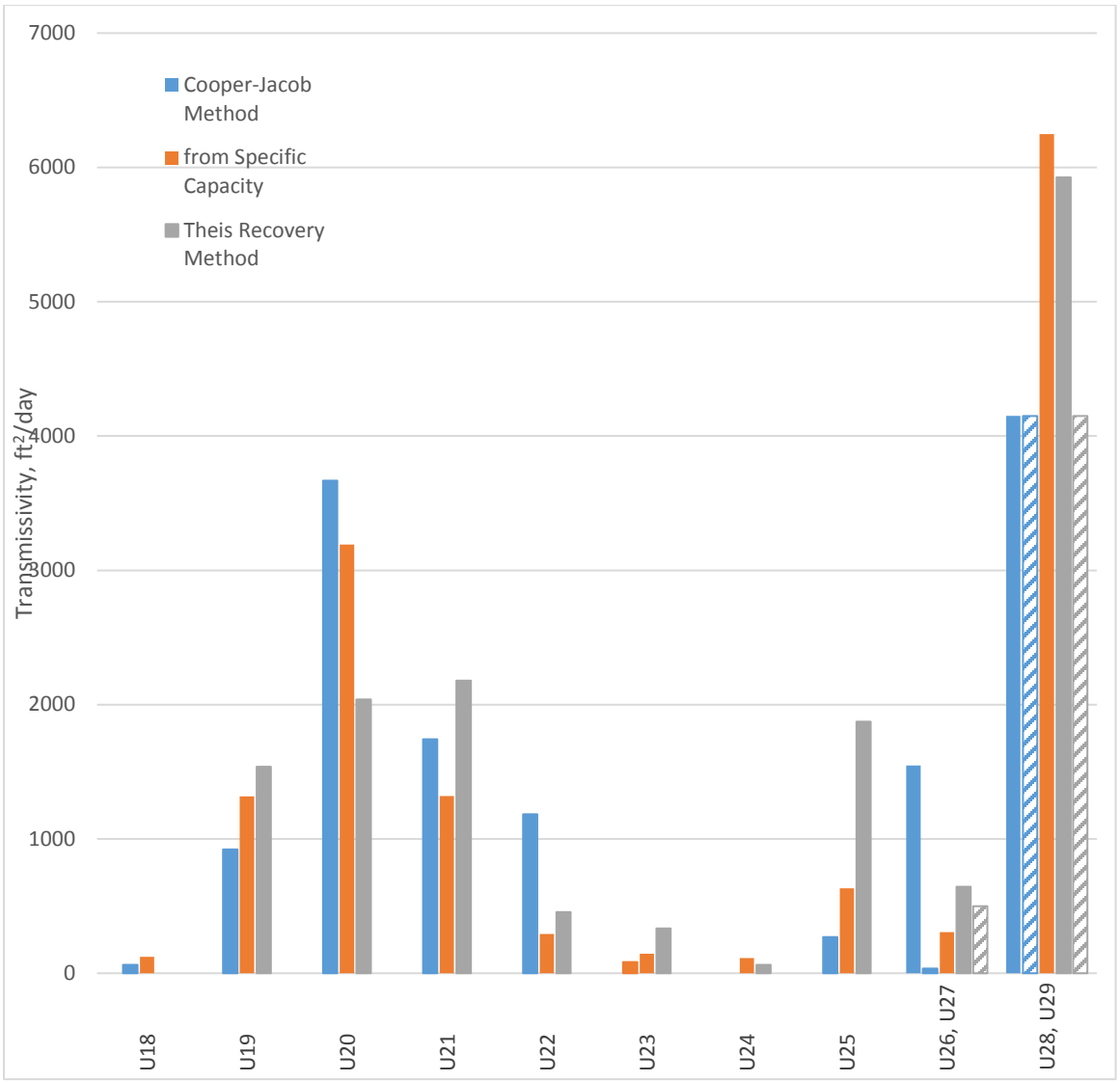

Figure 7. Aquifer testing transmissivity results from wetland preserve monitoring wells (monitoring well locations shown in Figure 3), in square feet per day (ft^2/day) using different analytical solutions; hatched fill indicates estimate from observation well. The average transmissivity is approximately 1000 ft^2/day.

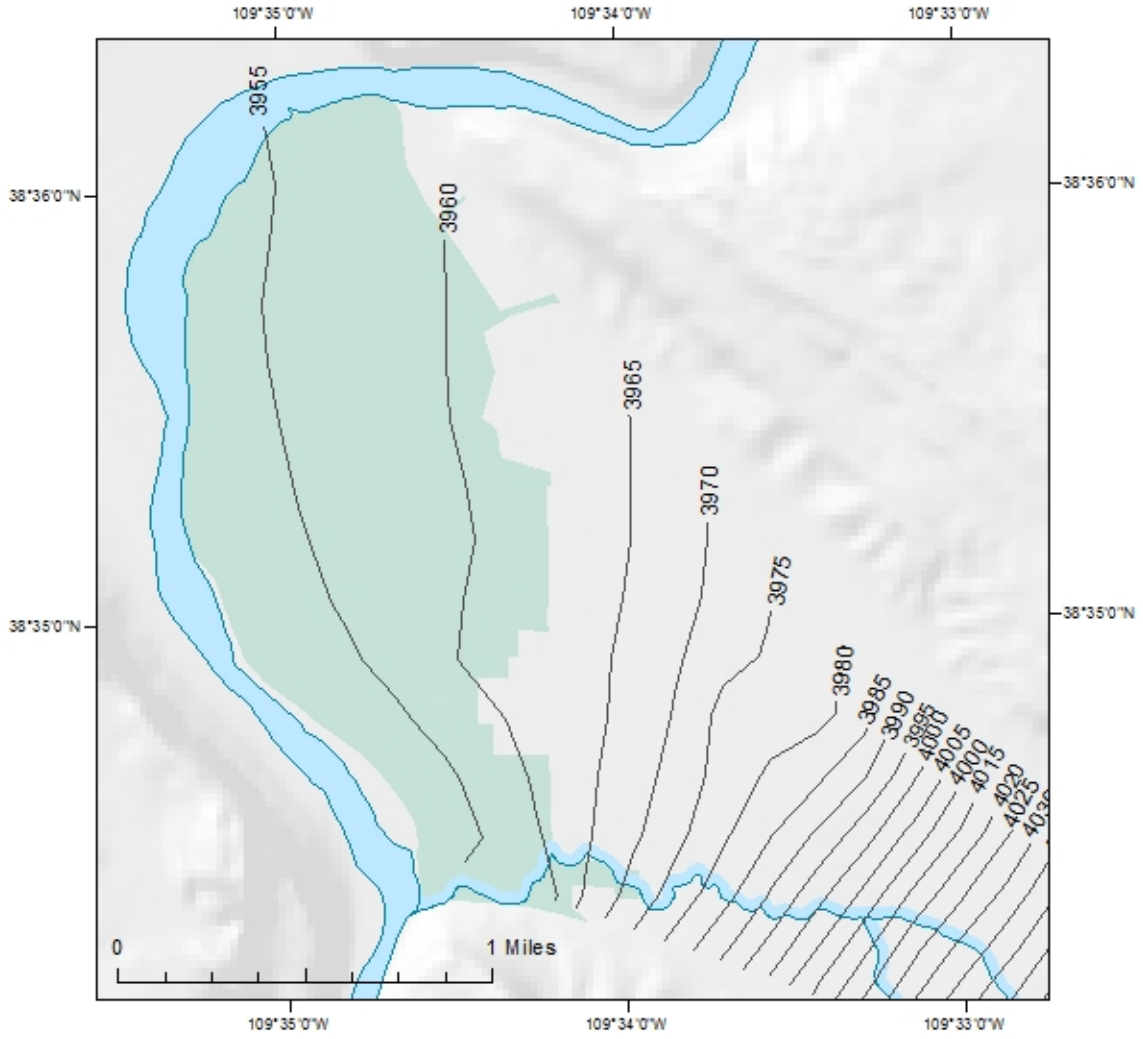

Figure 8. Potentiometric surface (water table) map showing groundwater flow generally to the northwest through the valley bottom toward the Colorado River. The potentiometric surface map was generated using water levels measured from alluvial wells; the contour interval is 5 feet. Given that groundwater flow is perpendicular to potentiometric surface contours, the map indicates that a large proportion of groundwater discharge to the Colorado River is occurring at the south end of the wetlands preserve, near Mill Creek.

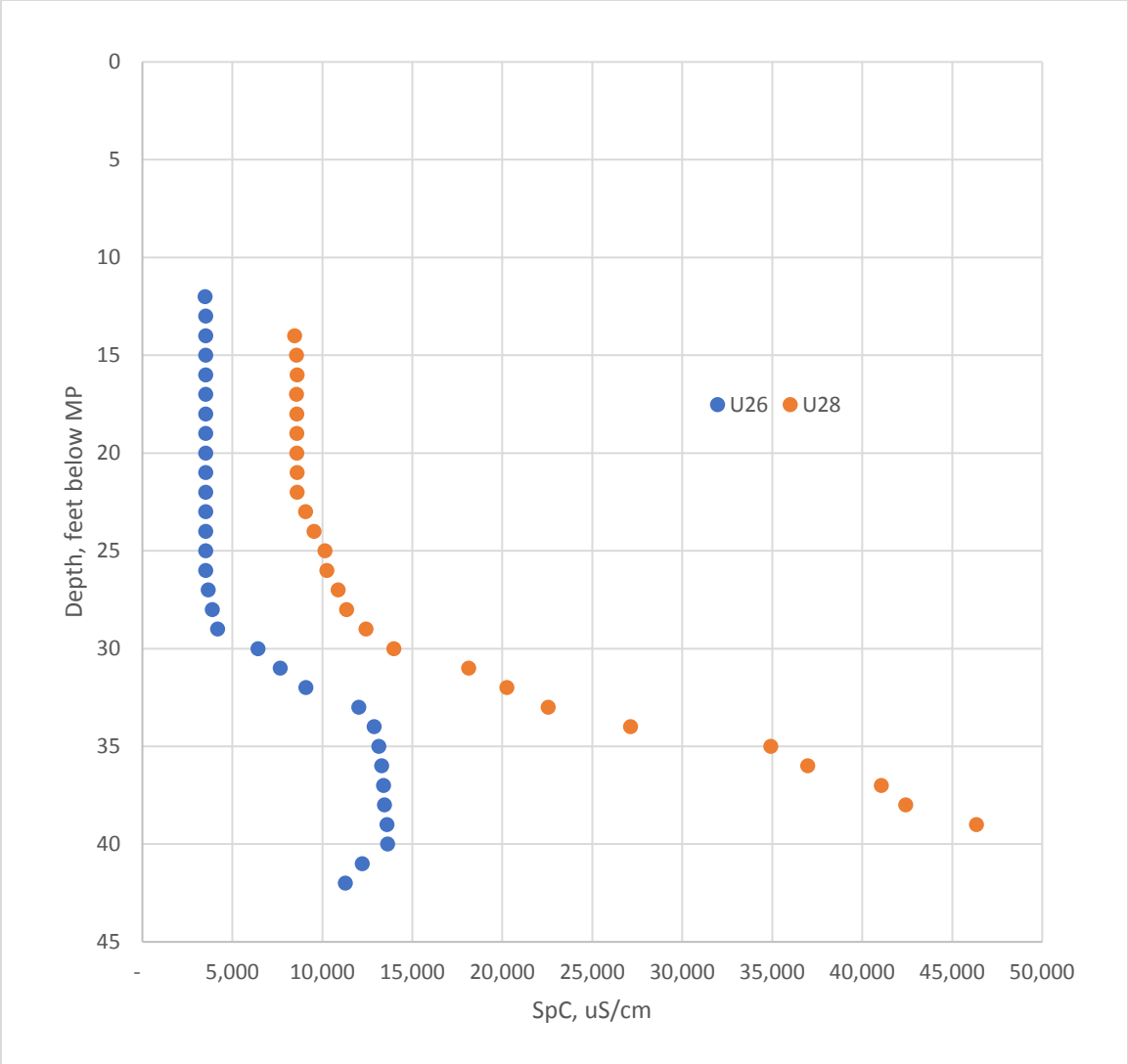

Figure 9. Graph displaying specific conductivity (SpC) profiles at U26 (blue) and U28 (orange); SpC values are shown in microSiemens per centimeter (µS/cm). The profiles indicate a transition from fresh groundwater to brine around 30 feet below the measuring point (i.e., top of the well casing).

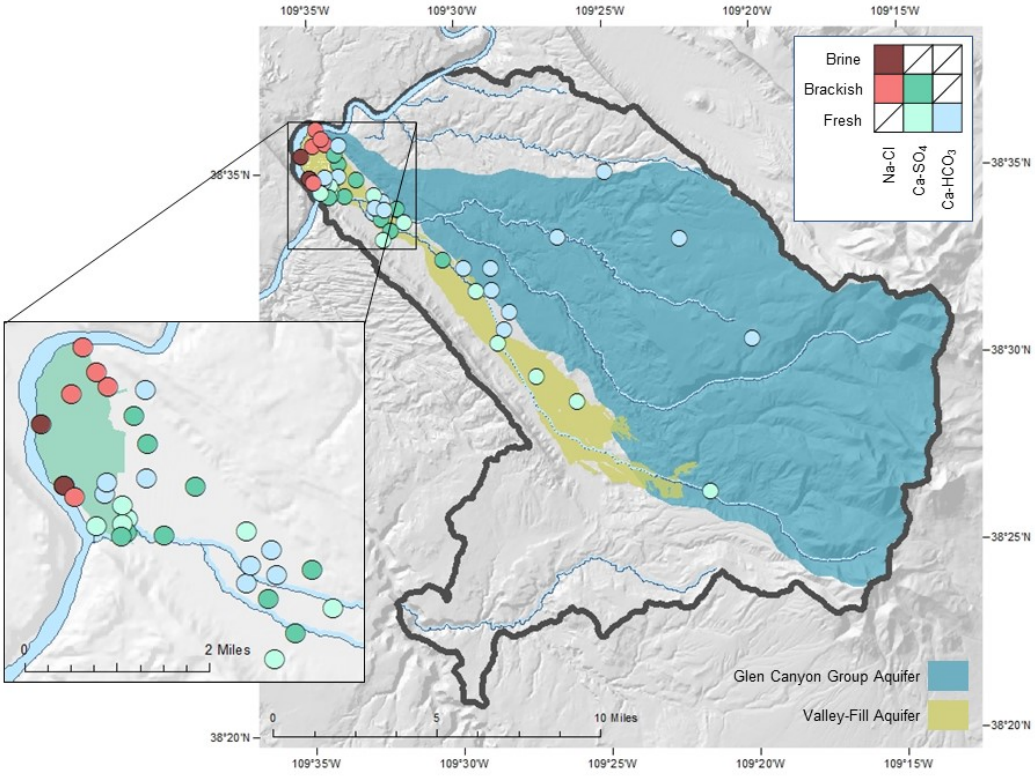

Figure 10. Map of groundwater hydrochemical type, based on major-ion chemistry. The three observed groundwater types include sodium chloride (Na-Cl, indicated in red), calcium sulfate ($Ca\text{-}SO_4$, green), and calcium bicarbonate ($Ca\text{-}HCO_3$, blue). Darker hues indicate higher total dissolved solids (TDS); brine is defined here as having greater than 100,000 mg/L TDS, brackish is less than 100,000 mg/L and greater than 1,000 mg/L, and fresh is less than 1,000 mg/L.

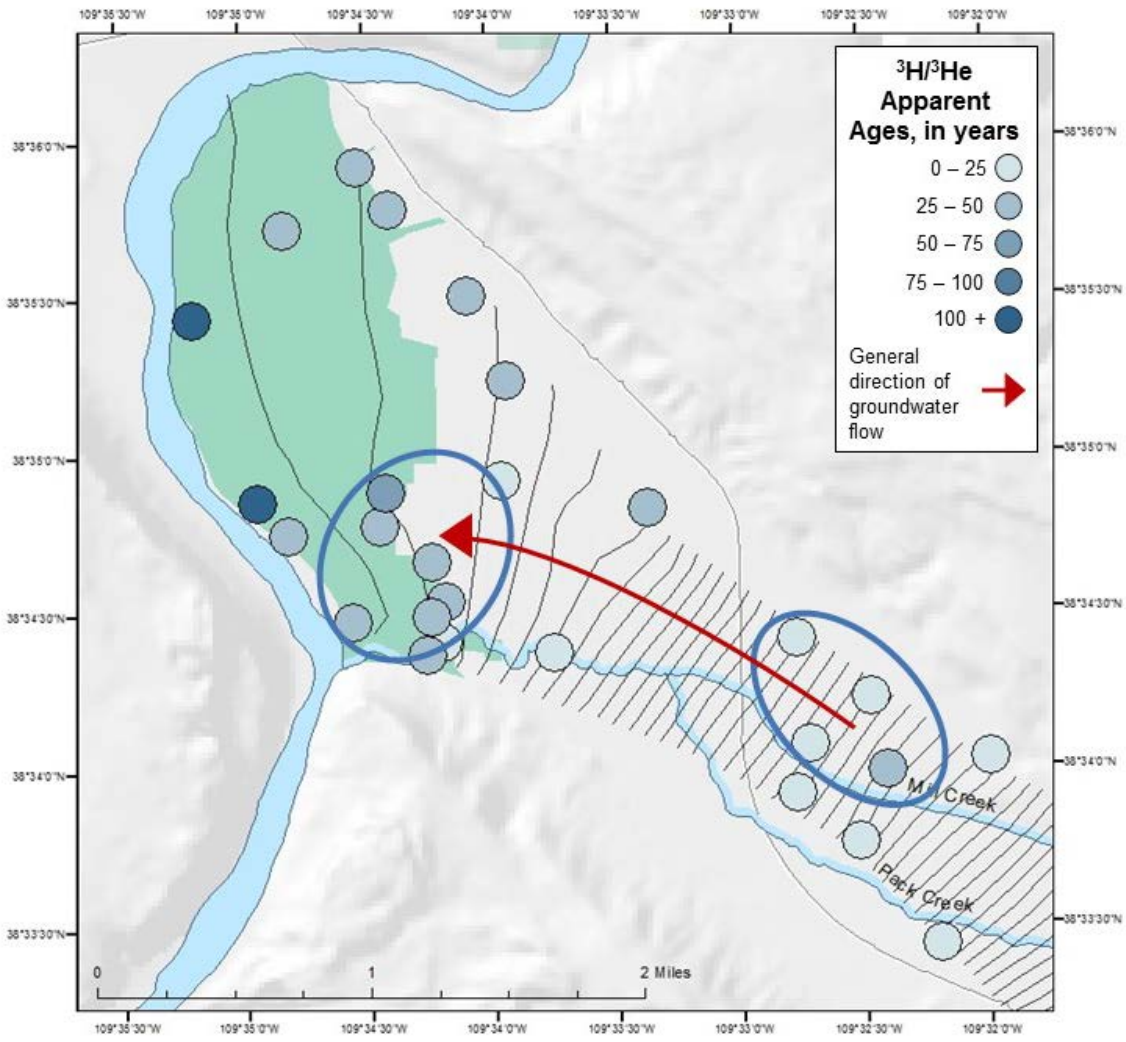

Figure 11. Map showing the tritium/helium-3 apparent ages from valley-fill aquifer samples (increasingly older samples are indicated by darker shades of blue), potentiometric contours (black lines) and groundwater flow direction (red arrow), and the sample groupings used to calculate a discharge rate to the Colorado River. The discharge calculation was performed by measuring the distance between the right and left sample groupings, and then dividing the distance by the age difference between the average age of each respective sample grouping.

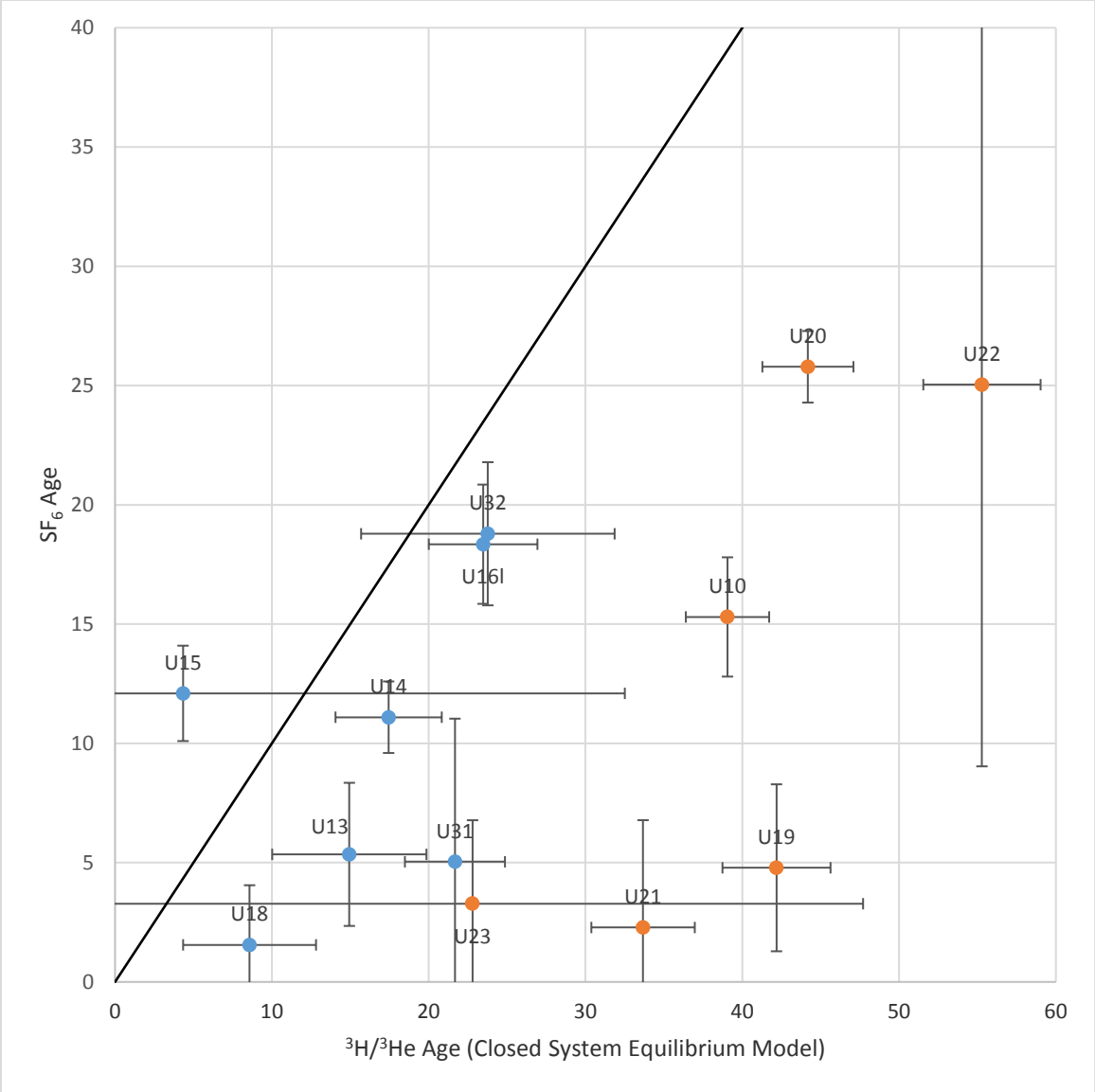

Figure 12. Plot showing the relationship between tritium/helium-3 and sulfur hexafluoride (SF_6) apparent ages. Samples collected more distant from the wetlands preserve (shown in blue) have calculated apparent ages that correlate closer to the tritium/helium-3 age 1:1 line compared to samples collected in or near the wetlands preserve (shown in orange). Many of the SF_6 samples collected were "contaminated," predominately those collected in the wetland preserve, as indicated by calculated apparent ages that were impossibly young (i.e., negative age). The results of this plot indicate that SF_6 contamination is spatially correlated with the wetlands preserve.

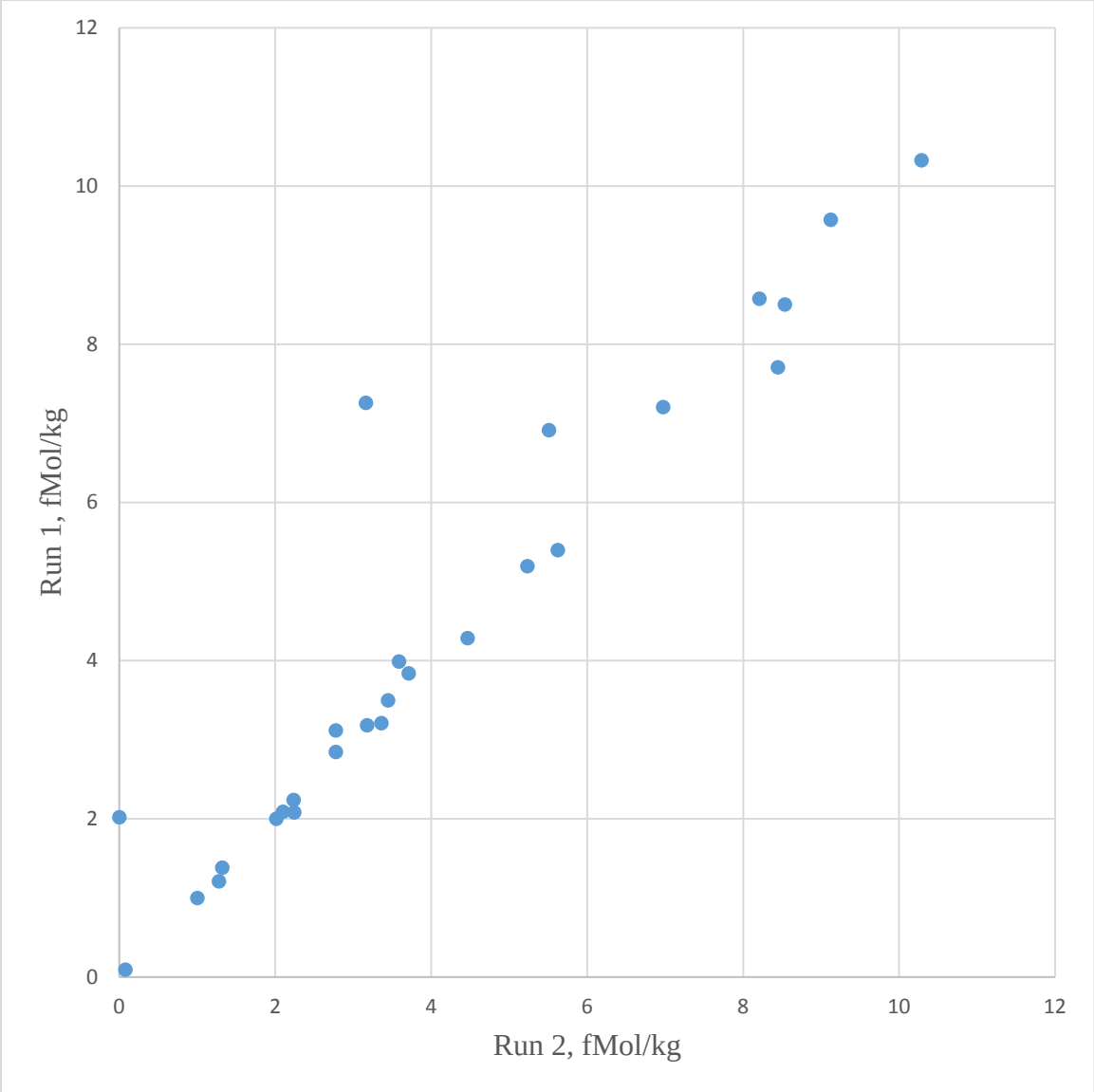

Figure 13. Graph showing replicate sulfur hexafluoride (SF_6) measured concentrations, shown in femtoMoles per kilogram (fMol/kg). In general, replicate concentrations are correlative, indicating that SF_6 contamination is not a result of measurement error.

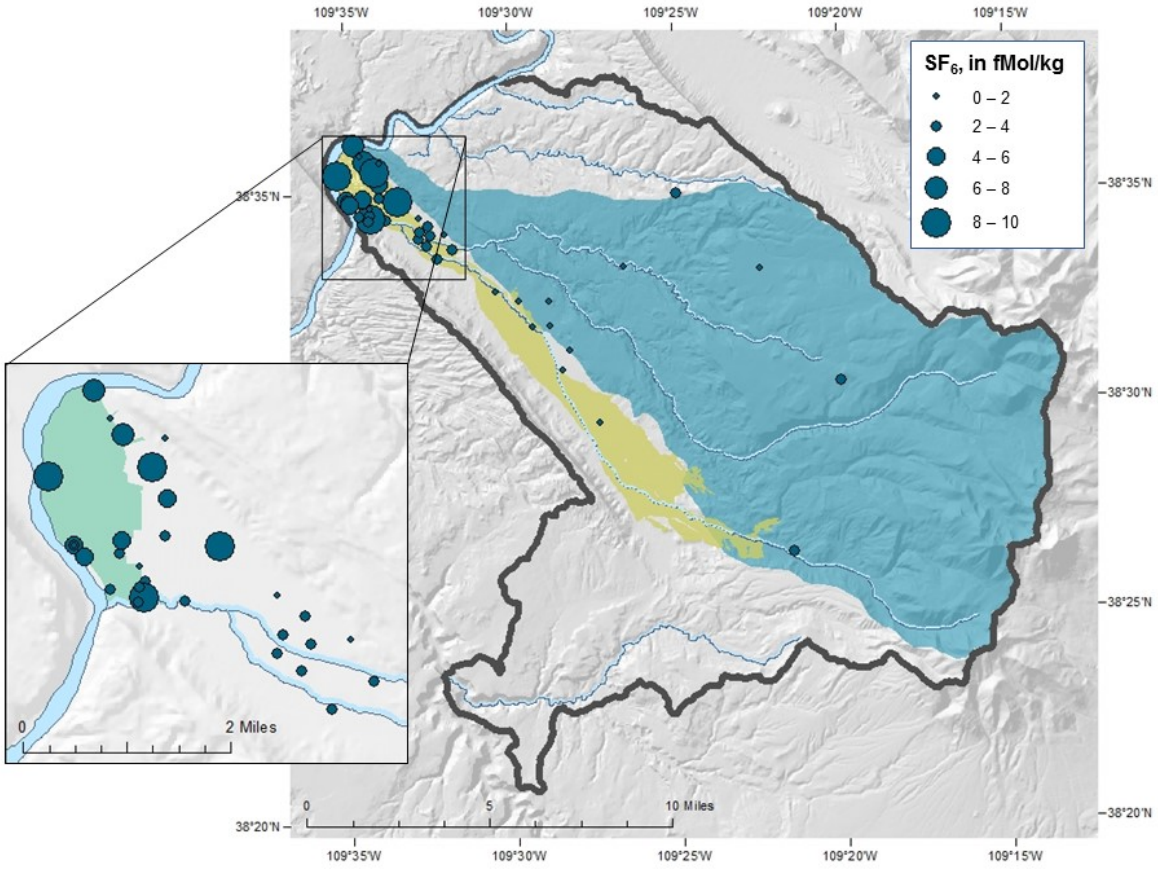

Figure 14. Study area map showing measured sulfur hexafluoride (SF_6) concentration in femtoMoles per kilogram (fMol/kg). Samples collected in and around the wetland preserve indicate SF_6 contamination, meaning that the SF_6 concentrations are above what is possible solely through atmospheric equilibration. The current atmospheric concentration of SF_6 is approximately 2 fMol/kg.

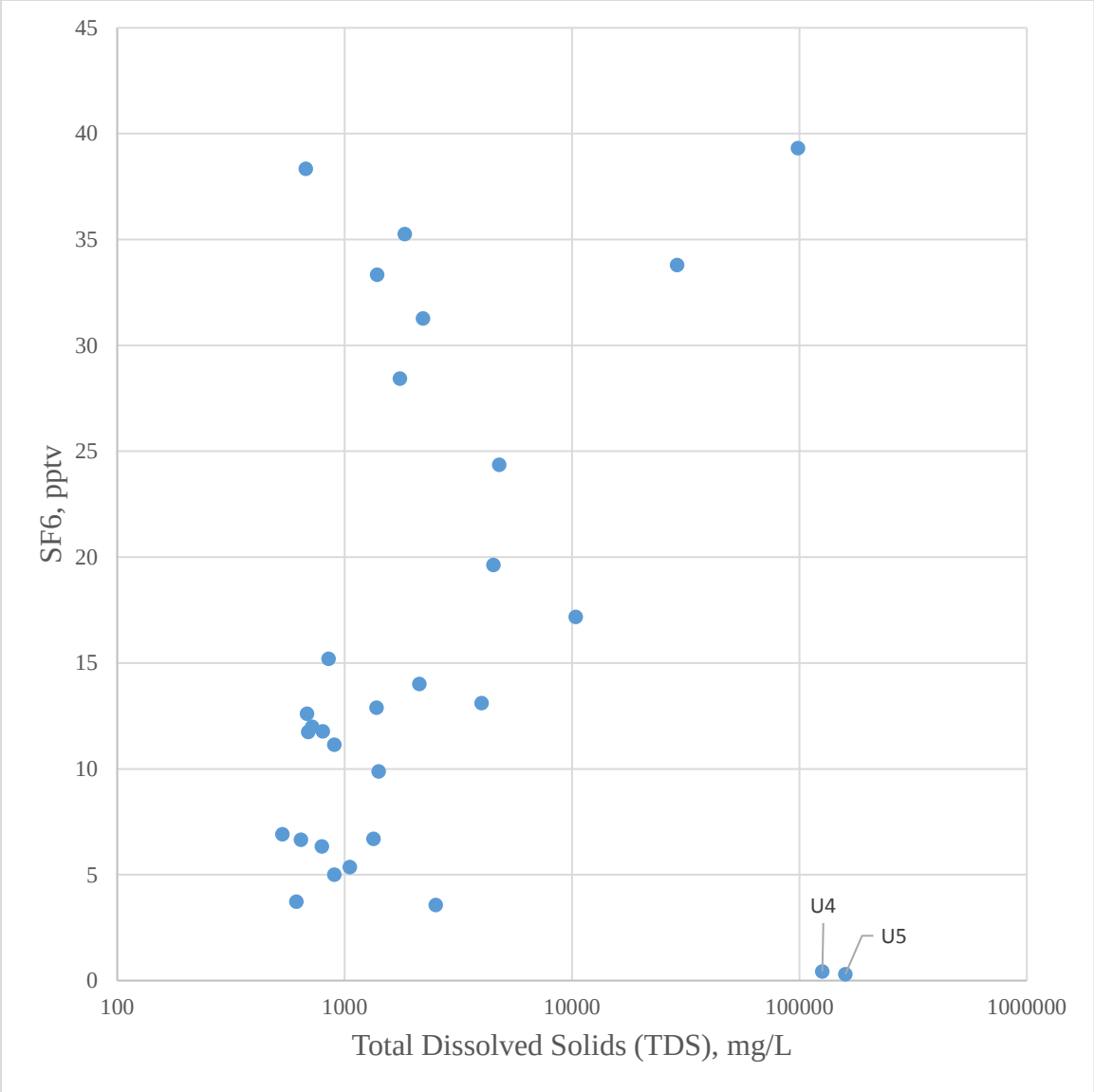

Figure 15. Plot comparing the calculated sulfur hexafluoride (SF_6) partial pressure, in parts per trillion by volume (pptv), to total dissolved solids (TDS), in milligrams per liter (mg/L). The samples from U4 and U5, both located in the wetland preserve, have TDS concentrations exceeding 100,000 mg/L (i.e., brine), and essentially no SF_6. This finding suggests that the observed SF_6 contamination is not inherently associated with brine, but rather to an unknown anthropogenic or terrigenic contamination source.

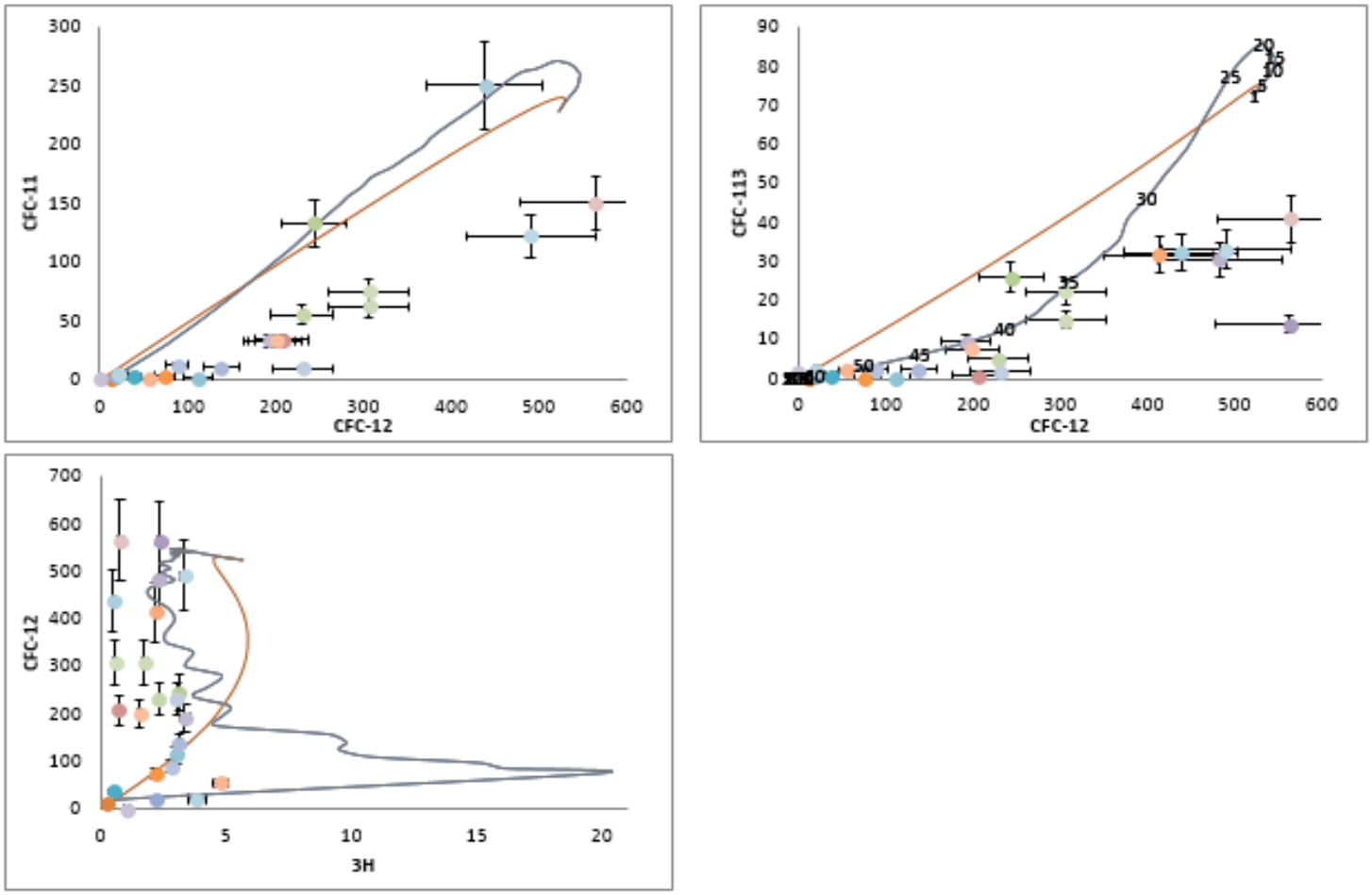

Figure 16. Tracer-tracer plots show concentrations of two tracers in relation to the PFM (piston flow model, blue line) and EMM (exponential mixing model, red line). The top left diagram shows that, generally, CFC-11 is degraded relative to CFC-12. Top right shows that CFC-113 is also degraded relative to CFC-12, especially for younger samples. The bottom panel shows that older samples fall along the PFM or EMM mixing lines, and that the other samples may be captured by a binary mixing model (a tie-line between the PFM model and EMM model).

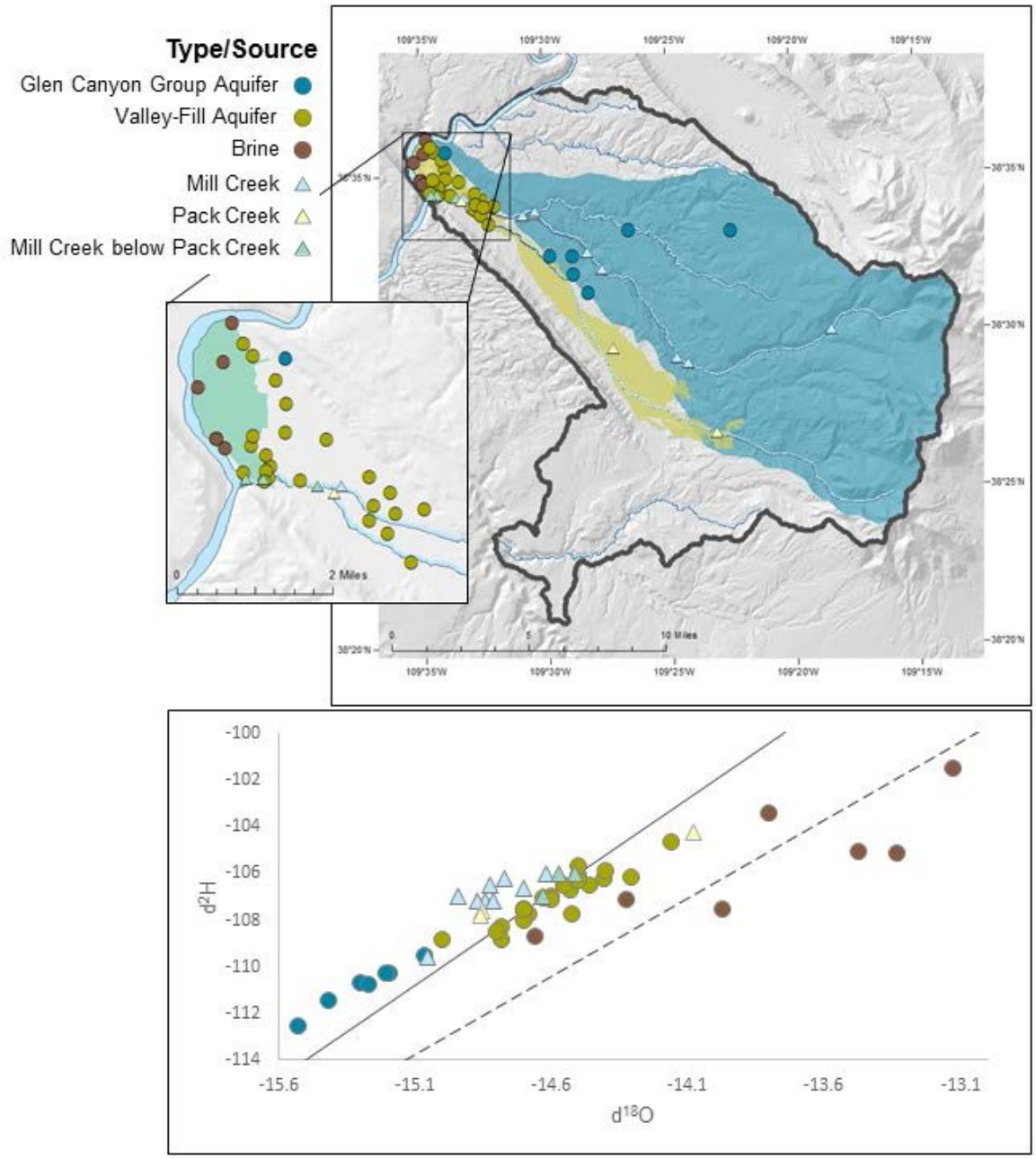

Figure 17. Stable isotope results. Upper Panel: Study area map showing oxygen and hydrogen stable isotope sampling locations. The symbols represent the type of water (e.g., groundwater versus surface water) collected at each location: Glen Canyon Group Aquifer, blue circle; valley-fill aquifer, green circle; brine, red circle; Mill Creek, blue triangle; Pack Creek, yellow triangle; and Mill Creek below the confluence with Pack Creek, green triangle. Lower Panel: Plot of stable isotope concentration (per mil) for hydrogen and oxygen; the solid line represents the global meteoric water line, and the dashed line is the Utah meteoric water line.

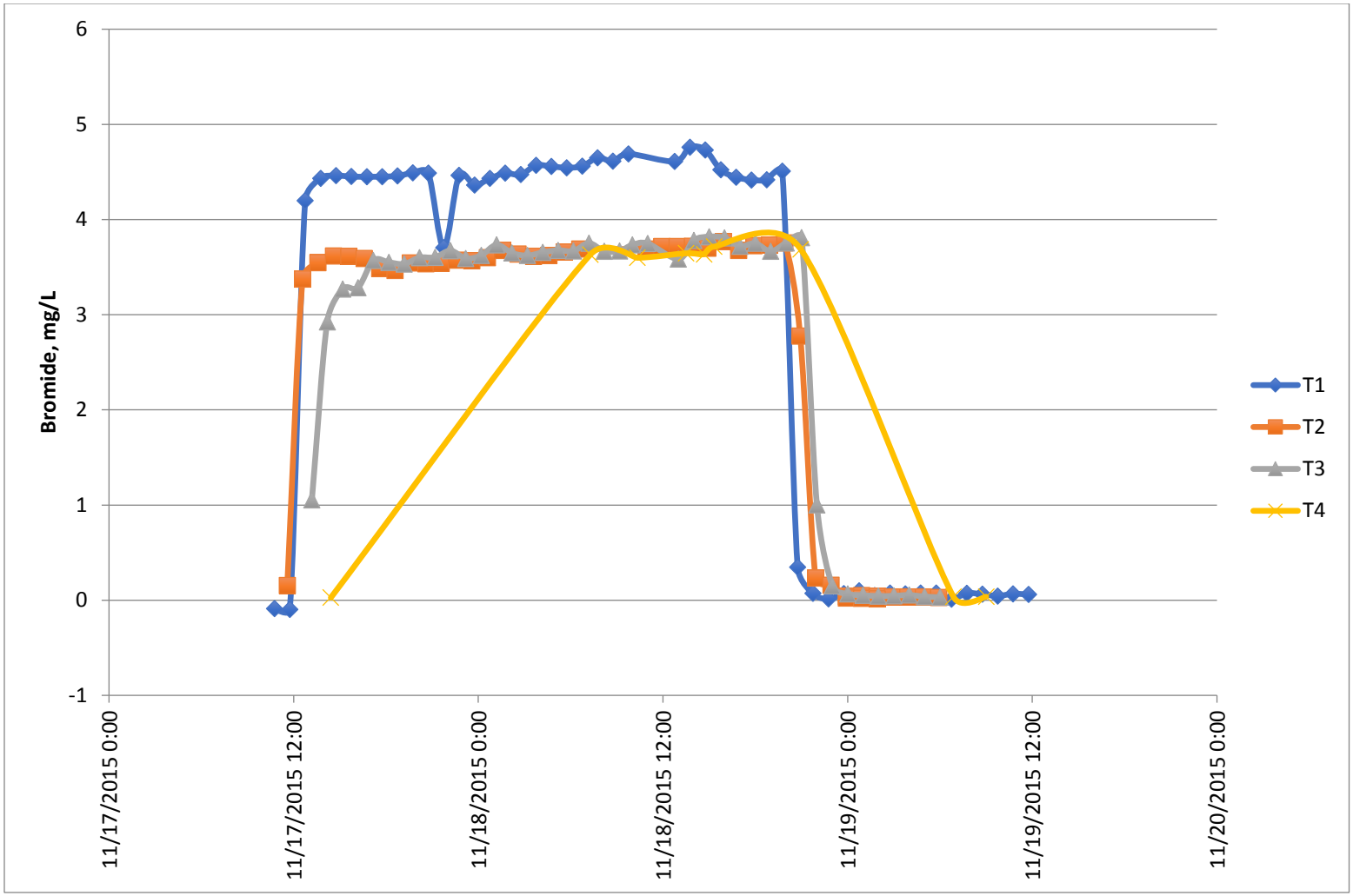

Figure 18. Establishing steady state at transport sites

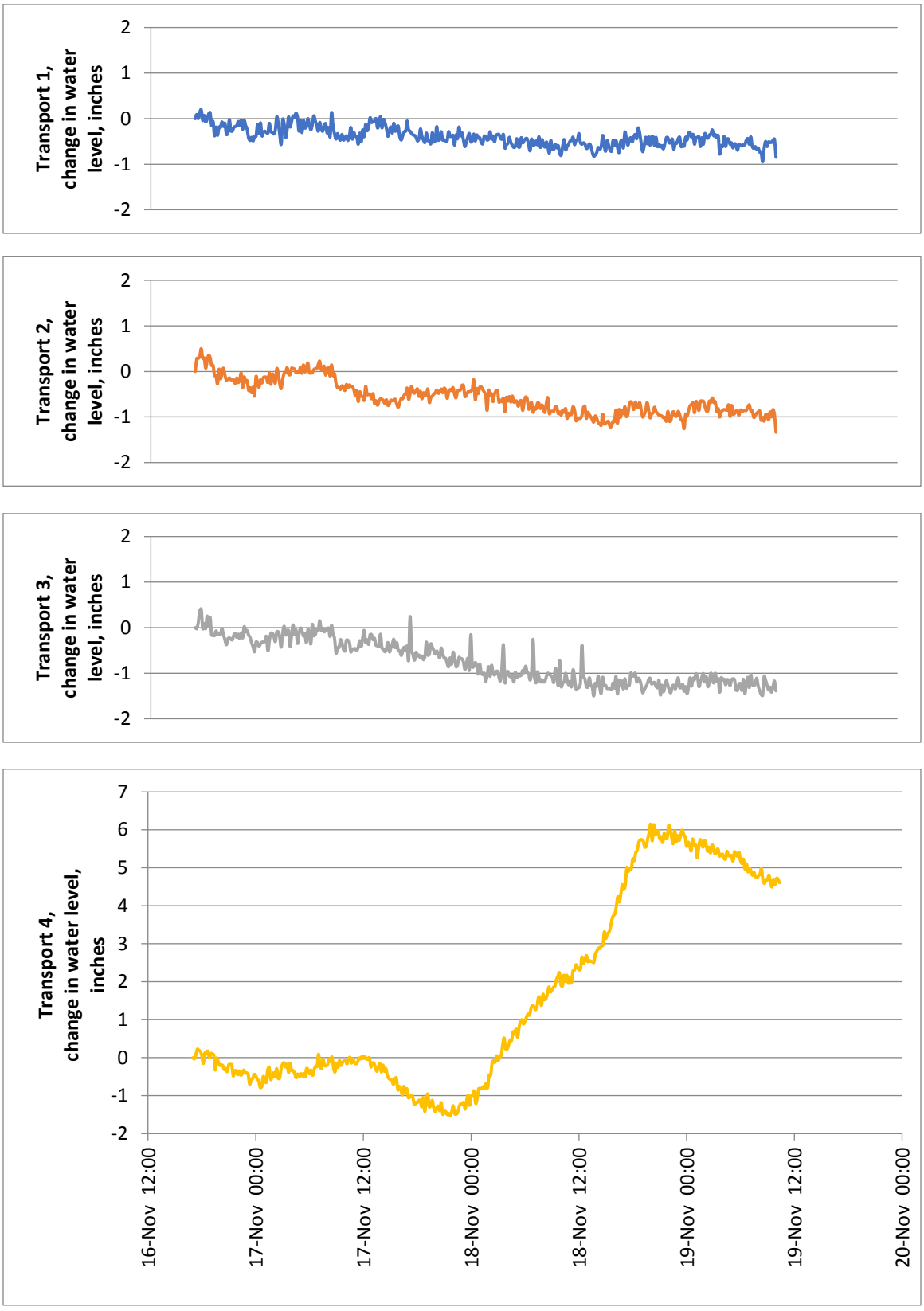

Figure 19. Transducer data

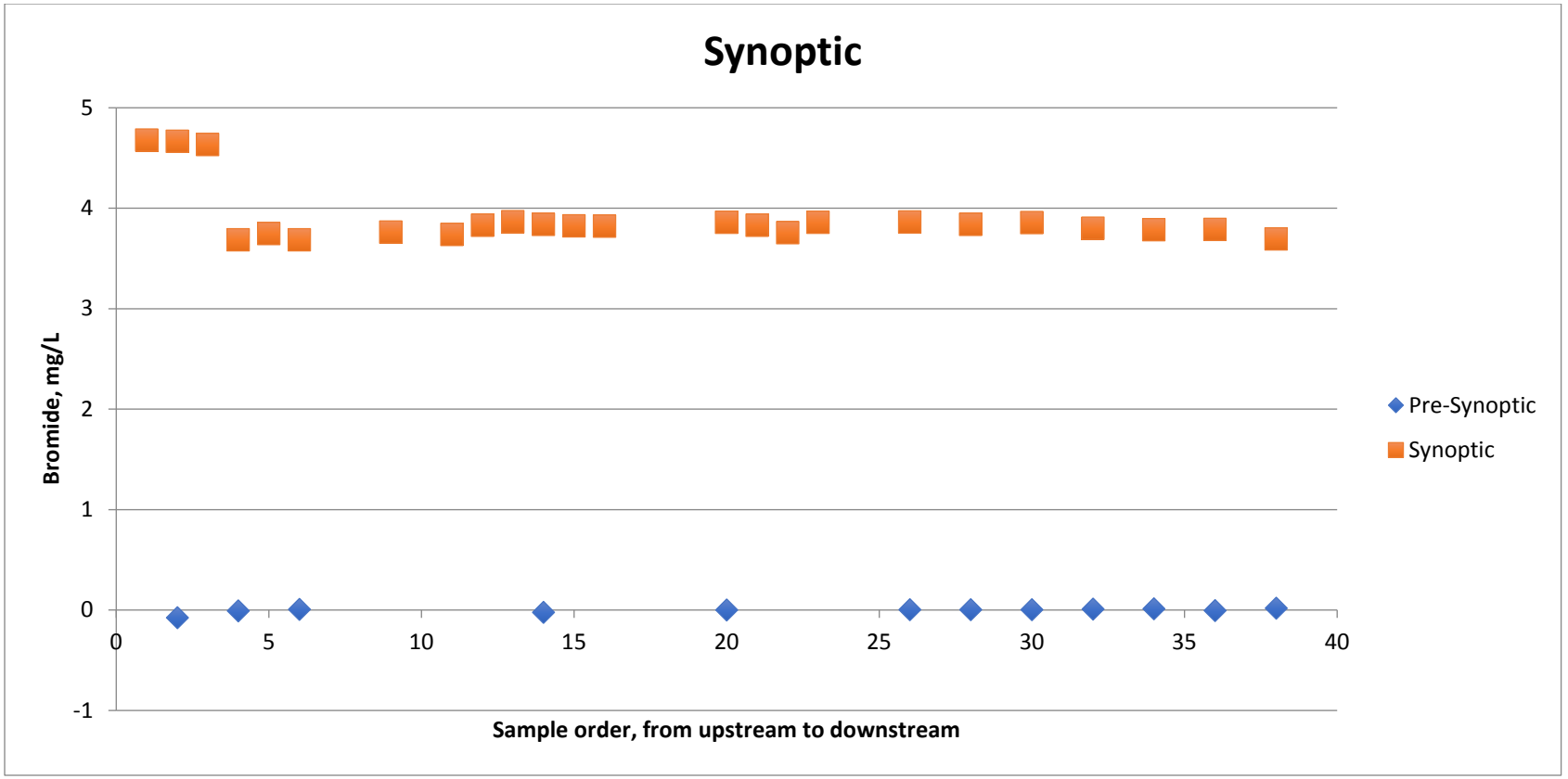

Figure 20. Synoptic

Table 1. Transmissivity results, square feet per day

Site ID	Cooper-Jacob method	Specific Capacity	Theis recovery method	Average	Standard Deviation
U18	60	120	—	90	30
U19	920	1300	1500	1300	250
U20	3700	3200	2000	3000	690
U21	1700	1300	2200	1700	350
U22	1200	290	460	640	390
U23	—	80, 150	340	190	100
U24	—	110	60	90	30
U25	270	630	1900	930	690
U26	30	310	640	330	250
U27 †	1500	—	500	1000	520
U28	4100	6200	5900	5400	920
U29 †	4100	—	4100	4100	0

† Observation well

Table 2. Field parameters and alkalinity

Site ID	Temperature	Specific Conductance	pH	Total Dissolved Gases	Dissolved Oxygen	Dissolved Oxygen	Alkalinity
	ºC	uS/cm		mmHg	mg/L	%	mg/L as $CaCO_3$
U1	16.6	30,535	6.6	740	0.2	3	255
U2	19.2	90,105	6.2	834	0.3	6	186
U3	16.2	11,930	7.2	750	0.3	4	300
U4	13.2	ODL	6.5	880	0.4	7	260
U5	13.7	ODL	6.2	1,274	0.1	2	165
U6	15.2	5,899	7.0	692	1.8	22	268
U7	16.8	1,092	6.8	680	3.5	45	270
U8	17.8	1,824	6.8	660	1.0	13	194
U9	16.1	2,115	7.0	800	1.8	21	124
U10	15.2	952	7.3	679	0.9	9	211
U11	15.7	680	7.0	720	1.5	18	300
U12	15.9	1,586	6.9	692	—	—	234
U13	15.9	1,574	6.9	685	—	—	216
U14	16.9	796	7.1	661	—	—	228
U15	17.5	1,519	6.9	682	—	—	216
U16	17.3	1,158	6.7	645	—	—	230
U17	16.6	998	6.7	694	—	—	314
U18	17.1	2,423	6.7	712	2.8	32	190
U19	15.4	987	7.2	700	0.3	4	180
U20	15.9	905	7.1	744	—	—	170
U21	14.3	921	7.0	691	7.7	86	273
U22	12.6	899	7.1	664	—	—	298
U23	16.9	3,581	6.6	712	1.1	13	174
U24	19.3	2,437	8.1	748	0.2	3	244
U25	13.6	3,306	7.0	760	2.9	33	310
U26	12.6	12,219	7.4	773	2.0	22	—
U27	12.7	1,223	6.8	676	4.5	48	183
U28	12.5	46,341	6.9	741	0.4	6	—
U29	13.4	5,188	7.0	727	1.2	12	216
U30	16.0	1,521	6.8	715	1.5	18	136
U31	16.3	906	6.6	682	0.1	2	275
U32	17.6	1,323	6.9	675	5.9	72	124

ODL, over detection limit

Table 3. Specific conductivity profiles at select sites

Depth BMP	**Specific Conductivity**	
feet	µS/cm	
	MW-09	MW-11
12	3,482	—
13	3,515	—
14	3,513	8,466
15	3,515	8,567
16	3,517	8,591
17	3,518	8,568
18	3,520	8,572
19	3,520	8,582
20	3,520	8,584
21	3,522	8,590
22	3,520	8,591
23	3,517	9,073
24	3,517	9,537
25	3,514	10,147
26	3,518	10,246
27	3,665	10,877
28	3,878	11,347
29	4,174	12,419
30	6,422	13,970
31	7,652	18,125
32	9,083	20,251
33	12,028	22,550
34	12,873	27,131
35	13,130	34,912
36	13,295	36,966
37	13,391	41,050
38	13,454	42,414
39	13,589	46,341
40	13,631	—
41	12,219	—
42	11,272	—

BMP, below measuring point
µS/cm, microSiemens per centimeter

Table 4. Major ion results

Site Name	Sodium	Potassium	Calcium	Magnesium	Chloride	Sulfate	Bicarbonate	TDS	Charge Balance
	mg/L	mg/L	mg/L	mg/L	mg/L	mg/L	mg/L	mg/L	%
U1	6,648	67	1,118	206	19,932	683	311	28,964	-23
U2	24,309	179	2,615	693	66,287	4,273	227	98,581	-22
U3	2,553	52	202	68	6,258	882	366	10,381	-22
U4	32,426	667	1,909	554	84,907	5,352	317	126,131	-23
U5	41,072	969	1,977	664	108,183	6,136	201	159,201	-24
U6	905	12	237	128	2,216	951	327	4,776	-17
U7	36	3	173	42	28	292	329	902	6
U8	27	4	325	82	32	1,131	237	1,838	-8
U9	30	4	382	106	54	1,405	151	2,131	-7
U10	23	2	142	45	24	302	257	795	3
U11	13	2	71	41	5	36	366	533	4
U12	79	4	181	82	48	704	285	1,382	-3
U13	59	4	204	78	48	754	263	1,411	-5
U14	32	3	86	39	24	181	278	643	0
U15	79	6	175	72	42	701	263	1,338	-5
U16	53	5	114	64	58	326	280	900	1
U17	29	3	162	28	32	167	383	802	5
U18	179	6	274	111	170	1,239	232	2,212	-6
U19	24	2	127	43	22	281	219	719	4
U20	17	2	117	42	22	209	206	613	9
U21	19	2	124	42	21	143	333	684	8
U22	20	2	116	42	19	112	363	674	7
U23	234	7	601	114	283	2,561	206	4,005	-13
U24	506	4	23	5	696	219	298	1,752	-10
U25	544	9	143	74	925	440	378	2,513	-5
U27	49	5	136	55	36	345	223	850	7
U29	1,104	13	195	68	2,264	605	263	4,511	-12
U30	37	3	260	52	56	816	166	1,391	-6
U31	27	2	125	33	17	152	335	691	5
U32	75	6	139	66	78	538	151	1,053	0

Table 5. Measured noble gas concentrations

Site ID	Neon	+ -	Argon	+ -	Krypton	+ -	Xenon	+ -	Helium-4	+ -	R/R_a †
	(ccSTP/g)	(ccSTP/g)	(ccSTP/g)	(ccSTP/g)	(ccSTP/g)	(ccSTP/g)	(ccSTP/g)	(ccSTP/g)	(ccSTP/g)	(ccSTP/g)	
U1	1.9E-07	4E-09	3.2E-04	9E-06	7.3E-08	4E-09	1.0E-08	5E-10	3.1E-07		0.209
U2	1.7E-07	3E-09	3.0E-04	9E-06	7.1E-08	4E-09	8.8E-09	4E-10	8.6E-06		0.088
U3	2.1E-07	4E-09	3.7E-04	1E-05	8.8E-08	4E-09	1.2E-08	6E-10	7.0E-07		0.149
U4	1.7E-07	3E-09	3.2E-04	1E-05	7.8E-08	4E-09	9.9E-09	5E-10	7.4E-06		0.071
U5	1.7E-07	3E-09	3.3E-04	1E-05	7.5E-08	4E-09	1.0E-08	5E-10	9.4E-06		0.067
U6	1.9E-07	4E-09	3.3E-04	1E-05	7.6E-08	4E-09	1.0E-08	5E-10	7.5E-08		0.529
U7	1.9E-07	4E-09	3.3E-04	1E-05	7.7E-08	4E-09	1.0E-08	5E-10	4.7E-08		1.014
U8	1.7E-07	3E-09	2.7E-04	8E-06	6.0E-08	3E-09	8.5E-09	4E-10	6.3E-08		1.123
U9	1.7E-07	3E-09	3.0E-04	9E-06	7.3E-08	4E-09	1.0E-08	5E-10	5.0E-08		1.677
U10	2.0E-07	4E-09	3.7E-04	1E-05	8.2E-08	4E-09	1.2E-08	6E-10	6.8E-08		1.168
U11	2.3E-07	5E-09	3.9E-04	1E-05	8.5E-08	4E-09	1.2E-08	6E-10	1.1E-07		0.490
U12	1.9E-07	4E-09	3.6E-04	1E-05	8.0E-08	4E-09	1.1E-08	6E-10	5.0E-08		1.013
U13	1.9E-07	4E-09	3.6E-04	1E-05	7.8E-08	4E-09	1.1E-08	6E-10	5.4E-08		0.948
U14	1.8E-07	4E-09	3.3E-04	1E-05	7.4E-08	4E-09	1.1E-08	6E-10	4.3E-08		1.098
U15	1.8E-07	4E-09	3.2E-04	1E-05	7.8E-08	4E-09	1.0E-08	5E-10	4.5E-08		0.932
U16	1.7E-07	3E-09	3.2E-04	1E-05	7.3E-08	4E-09	1.0E-08	5E-10	5.0E-08		1.040
U17	1.7E-07	3E-09	3.1E-04	9E-06	7.4E-08	4E-09	1.0E-08	5E-10	4.2E-08		0.995
U18	2.1E-07	4E-09	3.6E-04	1E-05	7.1E-08	4E-09	1.0E-08	5E-10	6.6E-08		0.826
U19	2.1E-07	4E-09	3.5E-04	1E-05	7.3E-08	4E-09	1.0E-08	5E-10	7.2E-08		1.135
U20	2.0E-07	4E-09	3.7E-04	1E-05	7.6E-08	4E-09	1.1E-08	5E-10	5.5E-08		2.053
U21	2.0E-07	4E-09	3.4E-04	1E-05	7.8E-08	4E-09	1.0E-08	5E-10	4.8E-08		1.792
U22	8.4E-07	2E-08	9.0E-04	3E-05	1.4E-07	7E-09	1.5E-08	7E-10	3.9E-07		1.096
U23	2.1E-07	4E-09	3.6E-04	1E-05	7.6E-08	4E-09	1.0E-08	5E-10	8.7E-08		0.650
U24	2.3E-07	5E-09	3.9E-04	1E-05	8.3E-08	4E-09	1.0E-08	5E-10	1.4E-07		0.468
U25	2.0E-07	4E-09	3.6E-04	1E-05	7.5E-08	4E-09	9.5E-09	5E-10	1.2E-07		0.439
U27	2.0E-07	4E-09	3.6E-04	1E-05	7.7E-08	4E-09	1.0E-08	5E-10	1.1E-07		0.641
U29	2.0E-07	4E-09	3.8E-04	1E-05	7.8E-08	4E-09	1.1E-08	6E-10	3.6E-07		0.333
U30	2.1E-07	4E-09	3.7E-04	1E-05	7.9E-08	4E-09	1.1E-08	5E-10	2.9E-07		0.322
U31	2.1E-07	4E-09	3.6E-04	1E-05	8.0E-08	4E-09	1.0E-08	5E-10	5.0E-08		1.248
U32	1.7E-07	3E-09	3.0E-04	9E-06	7.2E-08	4E-09	9.0E-09	4E-10	4.8E-08		0.941

† R/R_a, where R is the ratio of $^3He/^4He$ measured in the sample, and R_a is the ratio of $^3He/^4He$ in the atmosphere (1.384E-6)

Table 6. Closed-system equilibration (CE) model (Aeschbach-Hertig et al., 2000) results, assuming recharge elevation of 1500 m

Site ID	Recharge Temperature	Excess Air	Fractionation Factor	Sum of Chi Squared
	°C			
U1	12.1	0.001	0.00	2E-02
U2	16.3	0.119	0.94	2E+00
U3	8.7	0.029	0.74	5E-08
U4	13.0	0.130	0.95	8E-01
U5	11.6	0.134	0.96	6E-01
U6	12.9	0.048	0.84	8E-09
U7	13.6	0.132	0.86	1E-02
U8	19.0	0.001	0.00	6E-01
U9	12.4	0.001	0.00	5E-01
U10	10.0	0.070	0.81	2E-08
U11	11.3	0.062	0.70	1E-08
U12	11.1	0.143	0.85	7E-01
U13	11.8	0.141	0.84	7E-01
U14	9.8	0.000	0.00	3E-02
U15	12.2	0.051	0.92	2E-07
U16	13.0	0.131	0.93	4E-01
U17	12.5	0.017	0.93	8E-08
U18	15.7	0.132	0.75	6E-02
U19	16.6	0.125	0.73	2E-07
U20	13.2	0.138	0.79	8E-01
U21	16.3	0.128	0.78	1E-02
U22	30.0	0.153	0.13	2E-01
U23	15.7	0.133	0.75	2E-01
U24	18.6	0.130	0.64	2E+00
U25	17.3	0.127	0.75	3E+00
U27	15.1	0.133	0.77	4E-01
U29	12.1	0.143	0.79	2E+00
U30	14.8	0.137	0.73	4E-01
U31	14.9	0.134	0.76	9E-01
U32	15.1	0.116	0.80	3E-01

Table 7. Measured and calculated tritium results

Site ID	Tritium	+ -	R/Ra	Tritiogenic Helium-3	Terrigenic Helium-4	ΔNeon	Age	+ -
	TU	TU		TU	ccSTP/g	%	years	years
U1	0.49	0.03	0.209	4.80	2.69E-07	13	43	55
U2	0.29	0.03	0.088	163.32	8.56E-06	5	114	118
U3	2.23	0.09	0.149	14.60	6.57E-07	13	36	46
U4	0.27	0.03	0.071	65.84	7.31E-06	4	98	120
U5	0.01	0.09	0.067	68.60	9.37E-06	-9	164	154
U6	0.72	0.04	0.529	-3.35	3.01E-08	13	0 †	20
U7	3.12	0.13	1.014	0.14	-1.12E-09	25	1	4
U8	2.35	0.09	1.123	15.65	2.08E-08	16	37	3
U9	3.01	0.14	1.677	24.14	9.64E-09	6	39	2
U10	2.19	0.10	1.168	17.41	2.02E-08	17	39	3
U11	3.14	0.11	0.490	-0.52	5.86E-08	30	0 †	22
U12	1.59	0.08	1.013	4.31	6.67E-09	10	24	40
U13	2.33	0.11	0.948	0.91	3.93E-09	30	6	4
U14	2.31	0.10	1.098	1.66	-2.06E-09	10	10	21
U15	0.51	0.05	0.932	0.31	2.97E-09	6	9	6
U16	2.20	0.10	1.040	3.70	4.14E-09	12	18	4
U17	2.84	0.10	0.995	0.80	9.37E-10	-8	4	26
U18	1.34	0.11	0.826	2.89	1.68E-08	30	21	6
U19	1.73	0.13	1.135	18.69	2.44E-08	21	44	4
U20	3.36	0.24	2.053	36.36	6.87E-09	19	44	3
U21	3.82	0.35	1.792	19.63	-3.47E-09	36	33	3
U22	4.79	0.34	1.096	110.80	1.70E-07	347	57	4
U23	0.93	0.09	0.650	4.78	4.02E-08	20	33	0
U24	0.60	0.11	0.468	2.42	7.98E-08	46	29	26
U25	0.57	0.08	0.439	3.18	7.89E-08	19	34	27
U27	1.07	0.12	0.641	13.18	6.62E-08	16	46	8
U29	3.35	0.24	0.333	33.15	3.15E-07	15	43	16
U30	1.55	0.13	0.322	19.25	2.39E-07	14	47	23
U31	3.05	0.21	1.248	9.40	3.97E-09	18	25	3
U32	0.79	0.09	0.941	2.38	7E-09	9	25	8

Measured values: tritium, R/R_a; calculated values: $^3He_{trit}$, $^4He_{terr}$, ΔNe, age

† Computed negative ages are taken to be zero

Table 8. SF_6 results

Well ID	SF_6 Apparent Age	Apparent Recharge Year	Calculated mixing ratio	Measured concentration
	(years as of 2017)		(pptv)	(fMol/kg)
U1	C	C	25.63	10.29
U2	C	C	30.69	9.12
U3	C	C	10.73	5.23
U4	42.1	1973.5	0.35	0.12
U5	45.6	1970.0	0.23	0.08
U6	C	C	17.86	6.97
U7	1.6	2014.0	8.38	3.18
U8	C	C	26.19	8.53
U9	16.1	1999.5	4.55	4.47
U10	15.1	2000.5	4.69	2.10
U11	15.6	2000.0	4.57	2.24
U12	0	2017.0	9.42	3.71
U13	5.6	2010.0	7.15	2.78
U14	11.1	2004.5	5.59	2.24
U15	12.1	2003.5	5.43	2.02
U16	18.6	1997.0	3.91	1.32
U17	C	C	9.65	3.45
U18	C	C	20.96	8.45
U19	4.8	2011.5	7.57	3.18
U20	25.8	1990.5	2.54	1.00
U21	1.8	2014.5	8.64	3.36
U22	30.3	1986.0	1.68	3.16
U23	3.3	2013.0	8.15	3.19
U24	C	C	12.86	5.51
U25	Premodern	Pre-1953	-1.04	-0.39
U27	0	2017.0	9.36	3.59
U29	C	C	13.69	5.62
U30	C	C	20.02	8.21
U31	6.3	2010.0	7.12	2.78
U32	18.3	1998.0	4.17	1.28

"C" refers to "contaminated" samples, which have higher SF_6 than possible from merely equilibrating with the atmosphere prior to recharge

Table 9. Measured CFC results, pMol/kg

Site ID	**CFC-11**	**+ -**	**CFC-12**	**+ -**	**CFC-113**	**+ -**
	pMol/kg	pMol/kg	pMol/kg	pMol/kg	pMol/kg	**pMol/kg**
U1	0.051	0.005	0.151	0.005	0.003	0.004
U2	0.089	0.099	0.244	0.286	0.018	0.025
U3	0.066	0.021	0.090	0.004	0.003	0.004
U6	0.503	0.009	0.810	0.015	0.003	0.005
U7	1.904	0.024	0.924	0.098	0.113	0.002
U8	4.269	0.211	1.679	0.029	0.045	0.002
U9	0.029	0.003	0.451	0.002	0.000	0.000
U10	0.056	0.042	0.336	0.007	0.000	0.000
U11	0.172	0.130	0.583	0.090	0.385	0.647
U12	12.719	0.577	3.866	0.233	0.180	0.006
U13	0.878	0.011	0.951	0.010	0.024	0.001
U14	17.373	1.195	2.199	0.162	0.165	0.011
U15	3.863	0.025	1.780	0.005	0.152	0.001
U16	9.715	0.104	1.615	0.020	0.142	0.002
U17	0.194	0.001	0.352	0.003	0.011	0.008
U18	4.501	0.055	50.273	1.238	0.124	0.005
U19	0.769	0.714	1.014	0.860	0.055	0.055
U20	0.486	0.475	0.743	0.744	0.042	0.042
U21	0.381	0.565	1.017	1.642	0.140	0.229
U22	0.036	0.025	0.422	0.422	0.021	0.014
U23	1.348	0.027	69.709	1.294	0.035	0.001
U24	1.314	0.741	2.737	0.971	0.150	0.035
U25	0.892	0.826	0.984	0.003	0.079	0.047
U27	0.015	0.002	0.000	0.000	0.006	0.004
U29	1.891	0.067	1.993	0.028	0.155	0.010
U30	0.449	0.016	0.714	0.109	0.030	0.007
U31	0.134	0.004	0.822	0.050	0.008	0.011
U32	2.002	0.028	2.001	0.120	0.163	0.025

Table 10. Calculated CFC mixing ratios

Site ID	CFC-11	+ -	CFC-12	+ -	CFC-113	+ -
	pptv	pptv	pptv	pptv	pptv	pptv
U1	3.3	0.3	37.1	1.3	0.6	0.8
U2	1.5	0.1	12.4	0.2	0.0	0
U3	3.6	1.1	18.8	0.9	0.5	0.7
U6	34.0	0.6	207.2	3.8	0.8	1.1
U7	133.2	1.7	244.0	25.8	26.0	0.4
U8	390.1	19.3	563.1	9.8	13.9	0.7
U9	1.9	0.2	112.4	0.6	0.0	0
U10	3.2	2.4	74.6	1.6	0.0	0
U11	10.6	8.0	138.0	21.3	2.3	3.3
U12	776.6	35.3	903.8	54.4	35.7	1.1
U13	55.7	0.7	230.1	2.5	5.0	0.1
U14	989.7	68.1	483.2	35.5	30.4	2.0
U15	250.3	1.6	438.8	1.2	32.3	0.3
U16	657.0	7.0	413.8	5.0	31.7	0.5
U17	12.8	0.1	88.2	0.8	2.3	1.6
U18	350.2	4.2	14600.5	359.5	32.2	1.2
U19	62.7	58.2	306.9	260.2	15.0	15.0
U20	33.2	32.5	192.3	192.5	9.5	9.5
U21	4.4	0.01	20.6	14.9	2.3	0.3
U22	1.2	0.8	54.8	54.8	2.0	1.3
U23	104.7	2.1	20199.3	374.9	9.2	0.3
U24	118.0	66.5	903.9	320.5	72.1	46.7
U25	75.2	69.6	307.1	0.8	22.3	13.3
U27	1.1	0.2	0.0	0	1.4	1.0
U29	122.3	4.3	490.7	6.8	32.9	2.1
U30	33.5	1.2	199.6	30.4	7.4	1.8
U31	10.0	0.3	230.6	13.9	1.9	2.7
U32	150.8	2.1	564.8	33.9	40.8	6.3

Table 11. CFC apparent age results

	Recharge Year			Apparent Age (years)†					
Site ID	**CFC-11**	**CFC-12**	**CFC-113**	**CFC-11**	**+ -**	**CFC-12**	**+ -**	**CFC-113**	**+ -**
U1	1955	1960	1949	63	0.41	57	0.24	68	8.49
U2	1952	1953	1943	65	0.25	64	0.25	74	0.00
U3	1955	1956	1949	62	1.18	62	0.41	69	7.78
U6	1966	1974	1950	51	0.24	43	0.24	67	9.43
U7	1976	1976	1981	41	0.00	41	1.41	36	0.25
U8	2014	2014	1976	4	0.00	4	0.00	41	0.41
U9	1953	1969	1943	64	0.24	48	0.24	74	0.00
U10	1954	1966	1943	63	2.22	51	0.22	74	0.00
U11	1959	1970	1952	59	3.64	47	1.24	65	13.20
U12	2014	2014	1983	4	0.00	4	0.00	34	0.24
U13	1970	1975	1969	48	0.00	42	0.24	48	0.24
U14	2014	1991	1982	4	0.00	27	2.55	35	0.62
U15	1988	1987	1983	29	0.24	30	0.00	35	0.00
U16	2014	1986	1982	4	0.00	31	0.47	35	0.24
U17	1961	1967	1958	56	0.00	50	0.00	59	10.85
U18	2014	2014	1983	4	0.00	4	0.00	35	0.50
U19	1965	1988	1963	52	9.75	29	25.75	55	19.50
U20	1961	Pre-1940	1961	56	9.15	Premodern	—	56	17.75
U21	1956	Pre-1940	1963	62	0.00	Premodern	—	54	1.08
U22	Pre-1940	Pre-1940	1959	Premodern	—	Premodern	—	58	9.26
U23	1974	2014	1973	43	0.25	4	0.00	44	0.00
U24	1974	2014	1985	43	8.41	4	0.00	32	1.65
U25	1967	1980	1979	50	10.08	37	0.00	39	4.26
U27	1952	Pre-1940	1956	66	0.41	Premodern	—	61	9.31
U29	1975	1990	1983	42	0.25	27	0.75	35	0.50
U30	1966	1974	1971	51	0.25	43	1.48	46	1.68
U31	1960	1975	1952	57	0.24	42	0.85	65	12.49
U32	1978	2008	1984	39	0.25	9	9.53	33	1.03

† As of 2017

Table 12. Stable isotope results, permil

Site ID	$\delta^{18}O$	$\delta^{2}H$
	‰	‰
U1	-14.7	-109
U2	-14.0	-108
U3	-13.1	-101
U4	-13.5	-105
U5	-13.3	-105
U6	-14.3	-107
U7	-14.3	-106
U8	-14.8	-109
U9	-14.5	-108
U10	-14.8	-108
U11	-14.6	-107
U12	-14.4	-106
U13	-14.5	-107
U14	-14.6	-107
U15	-14.7	-108
U16	-14.5	-106
U17	-14.2	-105
U18	-14.4	-106
U19	-14.7	-108
U20	-14.6	-107
U21	-14.5	-106
U22	-14.5	-106
U23	-14.6	-107
U24	-14.8	-109
U25	-14.7	-108
U27	-14.7	-108
U29	-13.8	-103
U30	-14.7	-108
U31	-14.5	-106
U32	-15.0	-109

5 DISCUSSION

5.1 Conceptual Groundwater Model

The valley-fill aquifer is an unconfined aquifer situated in Quaternary alluvial and colluvial sediments that have accumulated in the elongated basin of Spanish Valley. The collapsed salt anticline valley cuts off the thick Glen Canyon Group sandstones that rim the sides of the valley; the cliff-forming valley walls form physical boundaries of the aquifer on its northeastern and southwestern sides. At the distal end of the system, the shallow brines create a boundary to freshwater flow and essentially mark the bottom of the freshwater, valley-fill aquifer.

Results of the electrical resistivity survey demonstrated, at least qualitatively, that the lens of fresh groundwater discharging to the Colorado River is thickest near Mill Creek, that brines are shallow in the north (i.e., the uppermost freshwater layer is thin or nonexistent), and that these are separated by a brackish transition zone in the middle (Figure 4).

The potentiometric surface map shows that groundwater discharging near Mill Creek comes from Spanish Valley, whereas groundwater discharging to the north comes from the springs and groundwater from the ridge (Figure 8).

The bromide tracer test indicated that essentially no groundwater (less than 0.1 cfs) is gained by Mill Creek in the wetland above the Colorado River. Valley-fill aquifer water must discharge either through evapotranspiration on the wetland or subsurface groundwater discharge to the Colorado River.

Gardner (2004) characterized the groundwaters in the wetland into three categories according to geochemical observations. He defined GCGA water as having $\delta^{18}O$ of -14.5 to -15.0 ‰, ^{3}H of less than 2 TU, and R/R_a less than 1; the valley-fill as having $\delta^{18}O$ of -14.0 to -15.0 ‰, ^{3}H of 6.5 to 17.5 TU, and R/R_a greater than 1; and the brine as having $\delta^{18}O$ of -13 to -13.5 ‰,

very low ^{3}H, and R/R_a less than 0.1.

Major ion chemistry reveals three geochemical water types: high-TDS sodium-chloride (brines), moderate-TDS calcium-sulfate, and low-TDS calcium-bicarbonate. Results indicate shallow brines in the wetland to the north and fresh groundwater near Mill Creek to the south, even at similar depths, corroborating the results of the electrical resistivity survey.

Outside the wetland, samples from deeper wells exhibit the calcium-sulfate signature typical of Pack Creek surface water, suggesting that loss from Pack Creek is a large contributor of recharge to the valley-fill aquifer. Steiger and Susong (1997) reported that upper Moab-Spanish Valley where Pack Creek comes into the valley was a significant recharge zone for the valley-fill aquifer, and Pack Creek is known to be a losing stream that is dry in the upper valley much of the year.

The low-TDS calcium-bicarbonate geochemical signature is observed in shallow wells on the north side of Pack Creek. GCGA waters are characterized by the low-TDS calcium-bicarbonate signature (Mill Creek above the valley is fed by GCGA groundwater); however, these samples lack environmental tracer compositions expected from GCGA groundwater. Many of the samples had high elevation $\delta^{18}O$ signatures; however, these waters do not have the "age" of GCGA water as given by ^{3}H, R/R_a, and $^{4}He_{terr}$.

Sumsion (1971) postulated that the valley-fill aquifer was recharged primarily by GCGA water from the northeast; however, we did not find significant amounts of "old" GCGA water in the valley-fill aquifer in lower Moab-Spanish Valley. The low-TDS calcium-bicarbonate samples could result from either loss from Mill Creek or runoff from GCGA springs along the northern valley wall whose dissolved noble gas signatures have had time to re-equilibrate.

5.2 Groundwater Discharge to Colorado River

Throughout the western United States, groundwater budgets rely heavily on groundwater discharge estimates, because in many systems, discharge is spatially focused and readily

measured (e.g., from wells, springs, or small streams). In Spanish Valley, some groundwater may be discharging directly into a very large river, the Colorado, whose flow is not measurably changed by Spanish Valley discharge.

Sumsion (1971) estimated that approximately 8,000 acre-feet of groundwater per year flowed to the Colorado River through the subsurface. Gardner (2004) used a Darcy Flux calculation along the length of the valley adjacent to the Colorado River to estimate between 100 and 1,500 acre-ft per year of groundwater discharge to the Colorado River. Two independent methods were implemented during this study to estimate the amount of groundwater entering the Colorado River from the subsurface, to follow up on the discrepancy between Sumsion (1971) and Gardner (2004). The first, the Darcy Flux method, uses transmissivity estimates from aquifer testing, the measured potentiometric surface, and the concept of flownet theory to estimate the amount of subsurface discharge to the Colorado using physical properties of the aquifer. The second method, the age gradient method, uses changes in apparent groundwater ages calculated from geochemical analyses of environmental tracers to calculate flow to the Colorado River, where the apparent age difference between samples gives us a direct measurement of the linear groundwater velocity along the flow path between sample sites.

5.2.1 Darcy Flux Method

Using Darcy's law alone, the cross-sectional area of flow is required to calculate discharge. Because the thickness of the aquifer is not well defined, flownet theory is applied. A flownet is a two-dimensional graphical representation of groundwater flow, valid for steady-state conditions. A flownet is constructed of equipotential lines (hydraulic head contours), which are perpendicularly intersected by flowlines (or streamlines). The flownet in Figure 18 was generated from known hydraulic head contours (see section 4.1.2) as upper and lower boundaries.

According to flownet theory, the total discharge through a flownet is calculated by

$$Q = T\Delta H n_{flowtubes} \quad (16)$$

where T is transmissivity, ΔH is the hydraulic head contour interval, and $n_{flowtubes}$ is the total number of flowtubes in the flownet.

Using a transmissivity of 1,000 ft^2/day (section 4.1.1), ΔH of 5 ft in a flownet that generates 8 flowtubes, the total discharge to the system (Q) is 40,000 ft^3/day, or approximately 300 acre-ft/year.

5.2.2 Age Gradient Method

Assuming piston flow, the apparent age difference between samples along the same flow path gives a direct measure of the average horizontal linear velocity (v) between those sample sites, given by

$$v = \frac{d}{\Delta T} \quad (17)$$

where d is the distance along the flowpath between sample sites, and ΔT is the age difference between samples.

Average linear velocity (v) is related to specific discharge (q) through porosity (n), by

$$q = vn \quad (18)$$

The age difference between samples (ΔT) was determined using two "clusters" of samples, approximately 2 miles apart (Figure 11). These samples were determined to be appropriately related because they lie along similar flowpaths and have similar geochemistry (Figure 10). Using ^{3}H/^{3}He apparent ages, the age difference between the upper and lower clusters was

determined to be 30 ± 14 years. The age difference was determined to be 28 ± 16 years using CFC-12 analysis. SF_6 apparent ages were discounted because of contamination (section 4.3.2), and CFC-11 and CFC-113 were discounted because of degradation and sorption, respectively (section 4.3.3). The distance was determined to be 9,000 ± 1,500 ft. The error quoted in the distance includes uncertainty introduced by spatial variations within a cluster of samples from which discharge was calculated.

Assuming a porosity (n) of 0.3, the resulting specific discharge (q) is 90 ± 45 ft/year for $^3H/^3He$, and 96 ± 48 ft/year for CFC-12. Assuming an aquifer width of 5,000 ft and thickness of 100 ft, the resulting volumetric discharges according to $^3H/^3He$ and CFC-12 apparent age data are approximately 1,000 and 1,100 acre-ft/year, respectively.

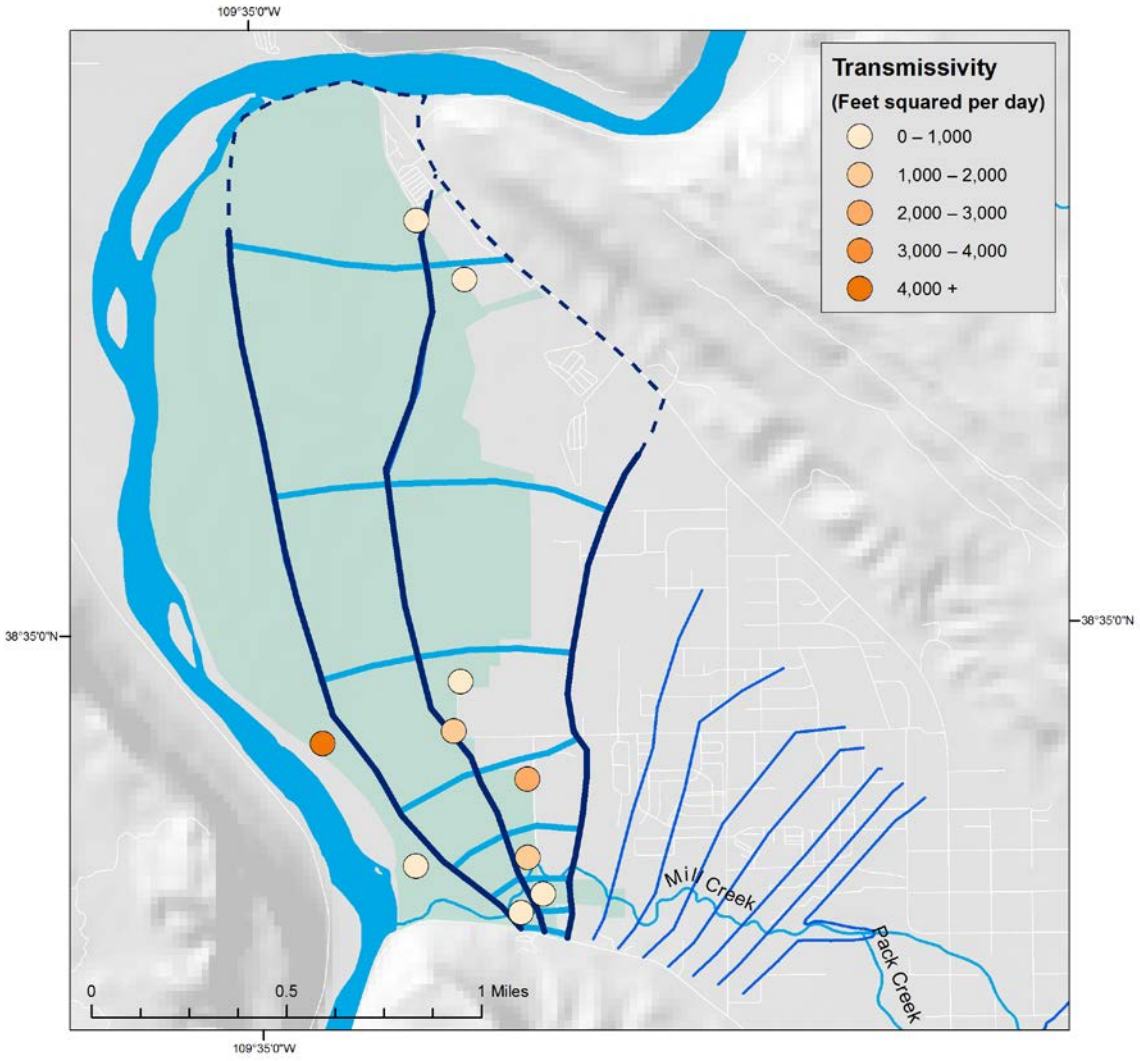

Figure 21. Map depicting a flownet used to calculate the Darcy flux discharge to the Colorado River through the wetland preserve. A flownet consists of equipotential lines (dark blue) and perpendicular flowlines (light blue); flowtubes are the regions between flowlines (eight total flowtubes).

6 CONCLUSION

Contrary to the conceptual model outlined by Sumsion (1971) that portrays the valley-fill aquifer as primarily recharged by GCGA water along the northern wall of the valley, we did not find "old" GCGA water in samples taken in the lower valley except for hints of mixtures that could contain modest amounts of GCGA water. Our data suggest that most of the GCGA water is discharging at the Moab City springs, and that the primary source of recharge to the valley-fill aquifer is surface water from Pack Creek and Mill Creek, which was precipitated at high elevation or at least above the study area.

Two independent methods were used to estimate the quantity of groundwater discharge in the wetland, either directly to the Colorado River or via evapotranspiration by wetland phreatophytes. The Darcy flux method yielded an estimate of approximately 300 acre-ft per year, while the age-gradient method yielded approximately 1,000 acre-ft per year. These estimates are significantly less than the previous estimate by Sumsion (1971) of 8,000 acre-ft per year, but agree with the estimates made by Gardner (2004) of 100 to 1,500 acre-ft per year.

The bromide tracer test indicates that less than 0.1 cfs of groundwater is escaping the flow system through Mill Creek above the Colorado River.

Our data indicate that the volume of water requested for water-rights transfer by the SJSVSSD does not exist in the valley-fill aquifer. Better understanding of the valley-fill aquifer system could be gained by gauging the streams that are the main inputs to the aquifer, Mill and Pack Creeks, to better constrain gains and losses.

APPENDIX A

BROMIDE TRACER TEST

A bromide tracer test was performed along Mill Creek near the Colorado River to evaluate whether groundwater was discharging into Mill Creek before reaching the Colorado River. The need for the tracer test was prompted by flow measurements taken with a SonTek FlowTracker Handheld-ADV (Acoustic Doppler Velocimeter) on an approximately 1-mile reach of lower Mill Creek (Figure 22) that indicated a gain of approximately 1 cfs. A bromide tracer injection was designed to locate and quantify the gain. A bromide tracer injection uses a concentrated solution of sodium bromide (NaBr) injected at a constant, known rate, whereby any dilution in measured concentrations of samples taken downstream indicates the occurrence of groundwater inflow (seepage) into the stream.

The bromide injectate was created by mixing six 55 lb bags of NaBr with approximately 60 gallons of water to create a solution with a concentration of approximately 500,000 mg/L. Stream measurements in the target area were approximately 9.8 cfs. The goal concentration for the samples was 3 mg/L. The pump rate was set to approximately 100 mL/min to achieve the target concentration (C_s) determined by following equation:

$$C_i X_i = C_s X_s \tag{19}$$

where C_i is the bromide concentration of the injectate, X_i is the rate of injection, C_s is the bromide concentration in the stream, and X_s is the maximum expected stream discharge.

An injection site was selected approximately one quarter mile upstream from the target area (Figure 23) to insure the injectate was fully mixed into the stream water before reaching the target area. A funnel was built using stream stones to funnel water just below the injectate to facilitate mixing in the rocky, shallow stream.

Three transport sites were established before the test to show when the bromide concentration in stream reached steady-state. At each site, an ISCO auto-sampler was set to collect a stream sample once every hour. Locations of the transport sites are shown in Figure 20.

A presynoptic was preformed to establish a baseline bromide concentration in the stream by identifying any natural sources of bromide; 12 presynoptic samples were collected. These values would be subtracted from synoptic values after analysis.

The solution was injected into Mill Creek at a constant rate for a duration of 30 hours. The bromide concentration in the stream reached steady state after approximately 4 hours, determined by time series of samples collected at four locations (transport sites) along the stream (Figure 18). After steady-state conditions were achieved, a synoptic of samples was collected at 24 locations along the stream.

After steady-state conditions were assumed to have been reached in the stream, a synoptic was taken where samples were collected from the same locations as in the presynoptic.

The samples were analyzed for bromide at the geomicrobiology lab at the University of Utah, in Salt Lake City, Utah. Samples were analyzed on a Metrohm 883 Basic IC Plus ion chromatograph at the Geomicrobiology Laboratory at the University of Utah in Salt Lake City, Utah. A standard was run every 10 samples, which allowed the concentrations to be corrected for instrument drift (Figure 24).

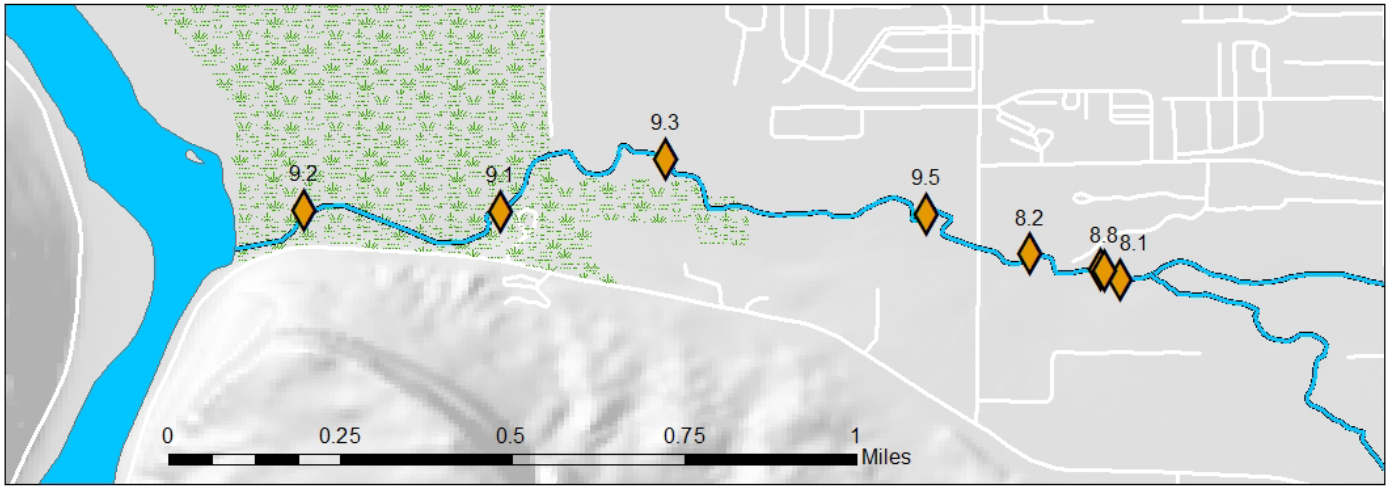

Figure 22. Flow measurements along Mill Creek that prompted the tracer test

Figure 23. Map of bromide tracer test; location of injection site, transport sites, pre-synoptic, and synoptic

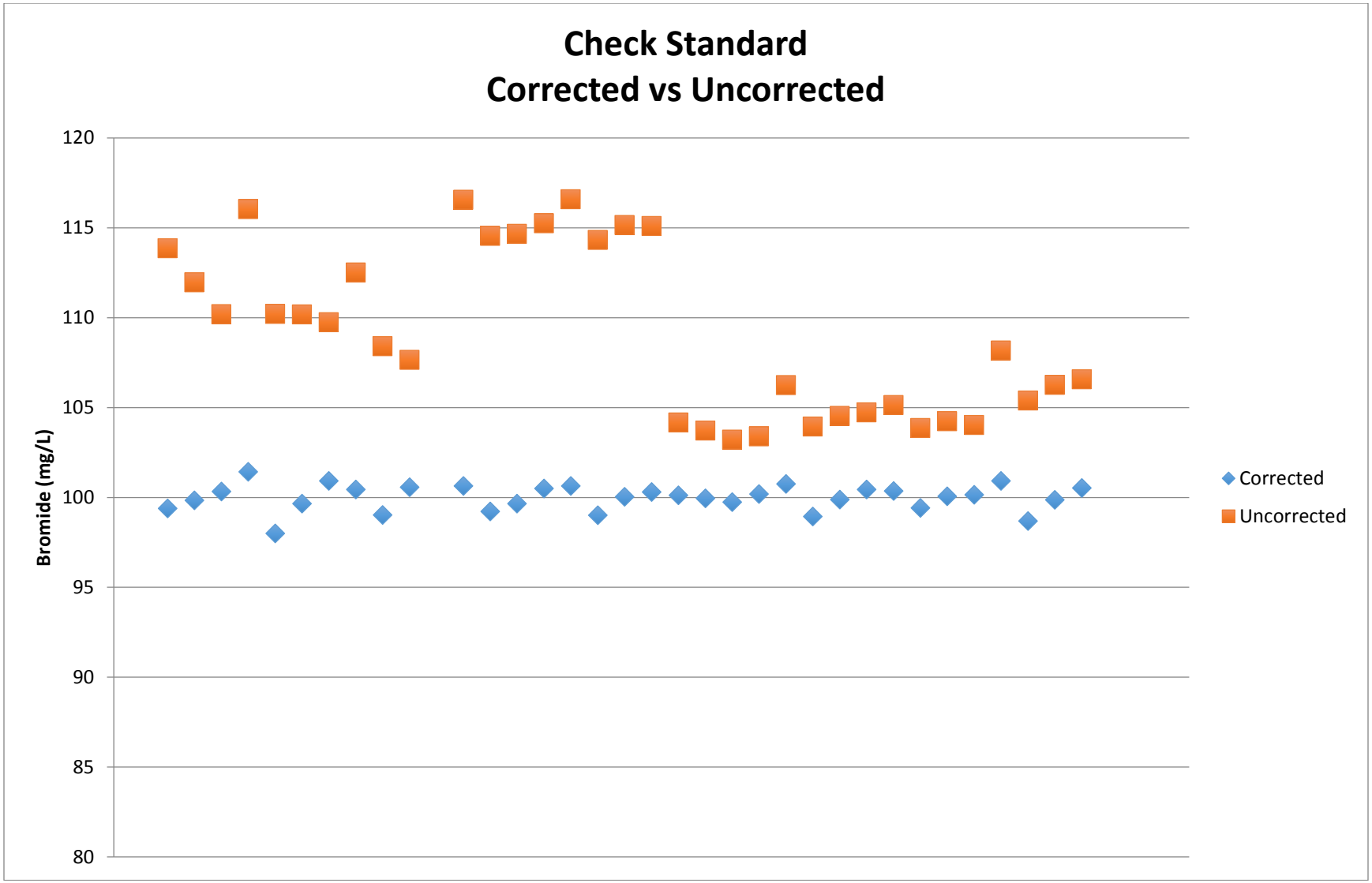

Figure 24. Sample correction (instrumental drift)

APPENDIX B

AQUIFER TESTING

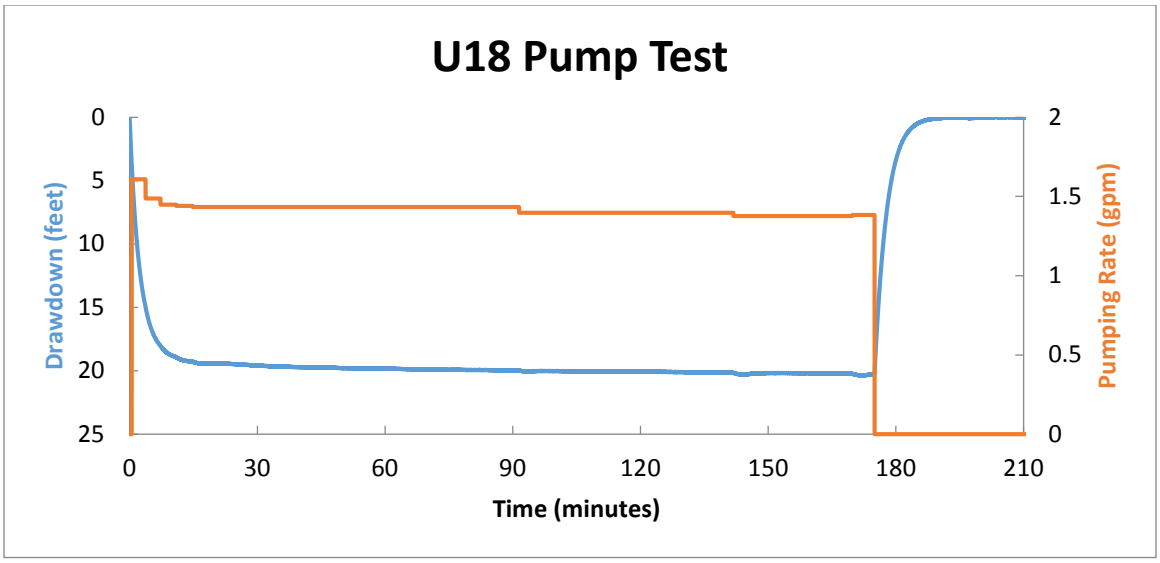
U18 Pump Test
Drawdown (feet)
0
5
10
15
20
25
Pumping Rate (gpm)
2
1.5
1
0.5
0
0
30
60
90
120
150
180
210
Time (minutes)

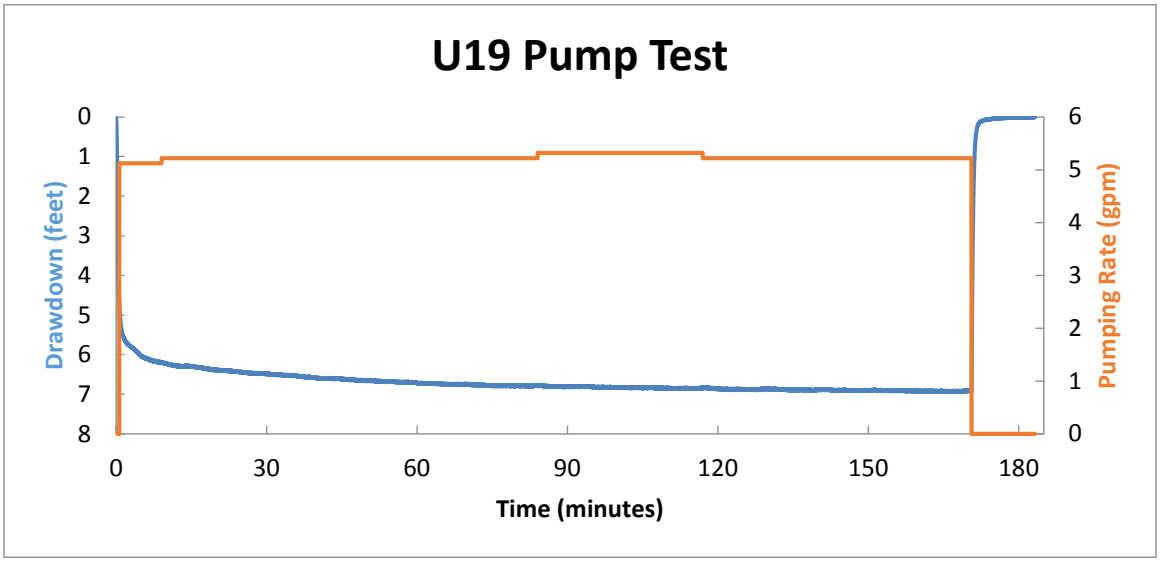
U19 Pump Test
Drawdown (feet)
0
1
2
3
4
5
6
7
8
Pumping Rate (gpm)
6
5
4
3
2
1
0
0
30
60
90
120
150
180
Time (minutes)

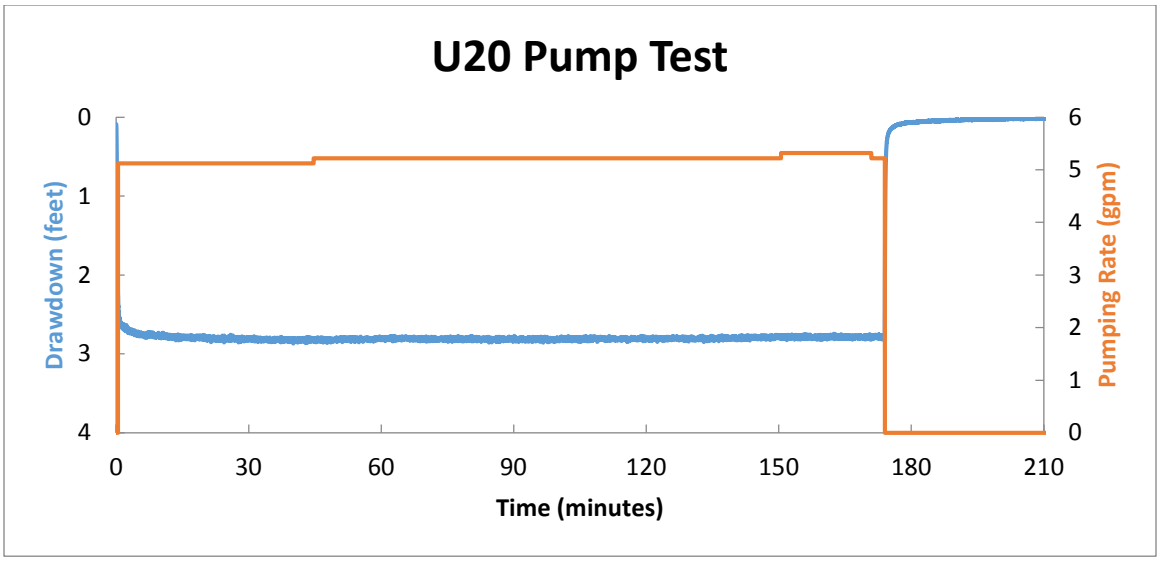
U20 Pump Test
Drawdown (feet)
0
1
2
3
4
Pumping Rate (gpm)
6
5
4
3
2
1
0
0
30
60
90
120
150
180
210
Time (minutes)

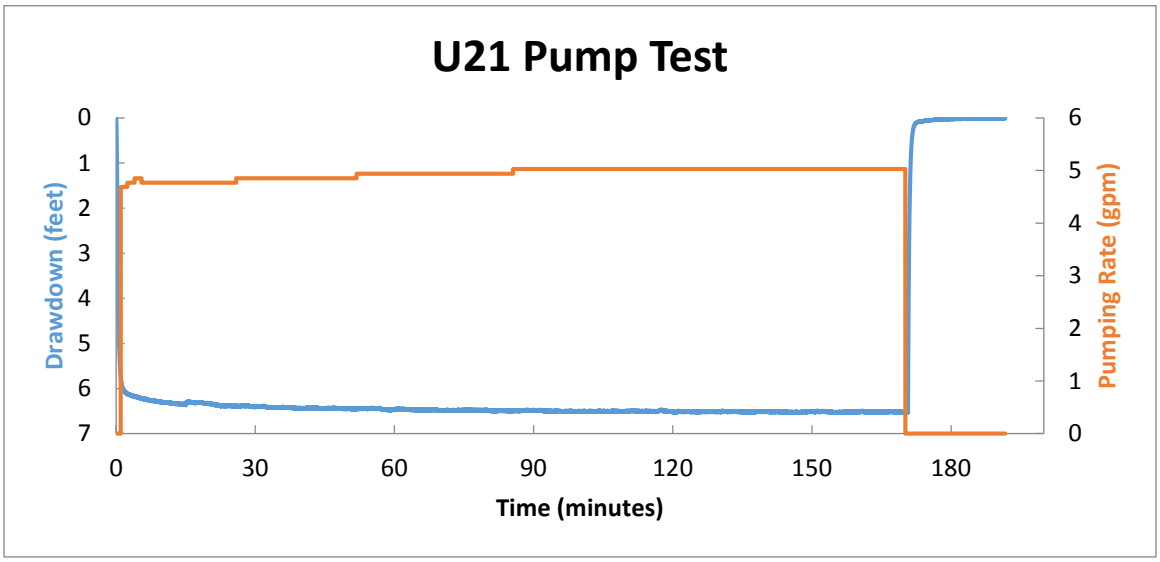
U21 Pump Test
Drawdown (feet)
0
1
2
3
4
5
6
7
Pumping Rate (gpm)
6
5
4
3
2
1
0
0
30
60
90
120
150
180
Time (minutes)

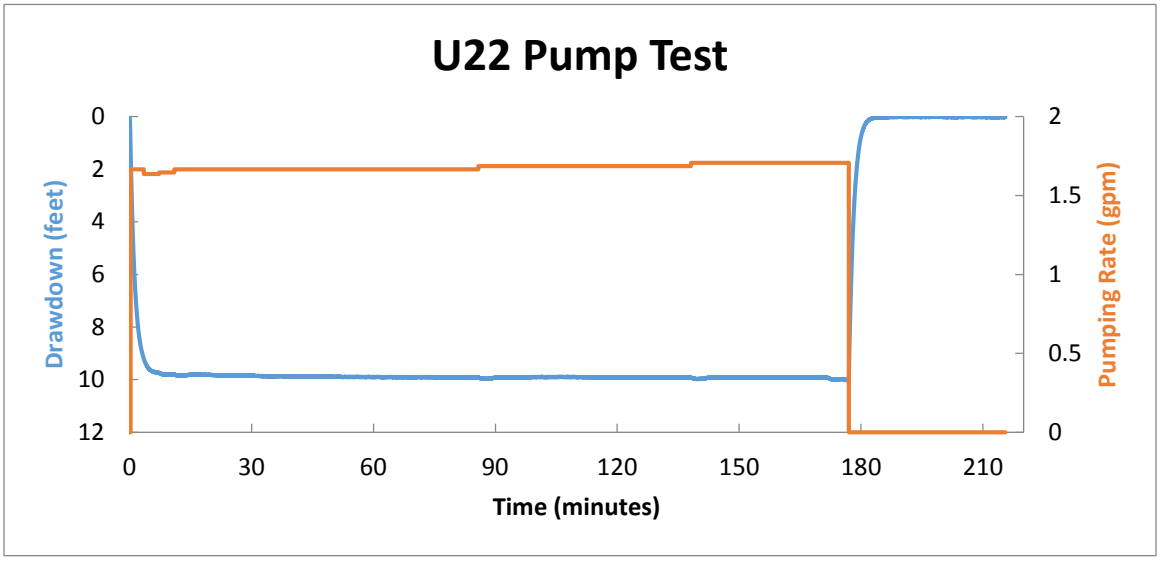
U22 Pump Test
Drawdown (feet)
0
2
4
6
8
10
12
Pumping Rate (gpm)
2
1.5
1
0.5
0
0
30
60
90
120
150
180
210
Time (minutes)

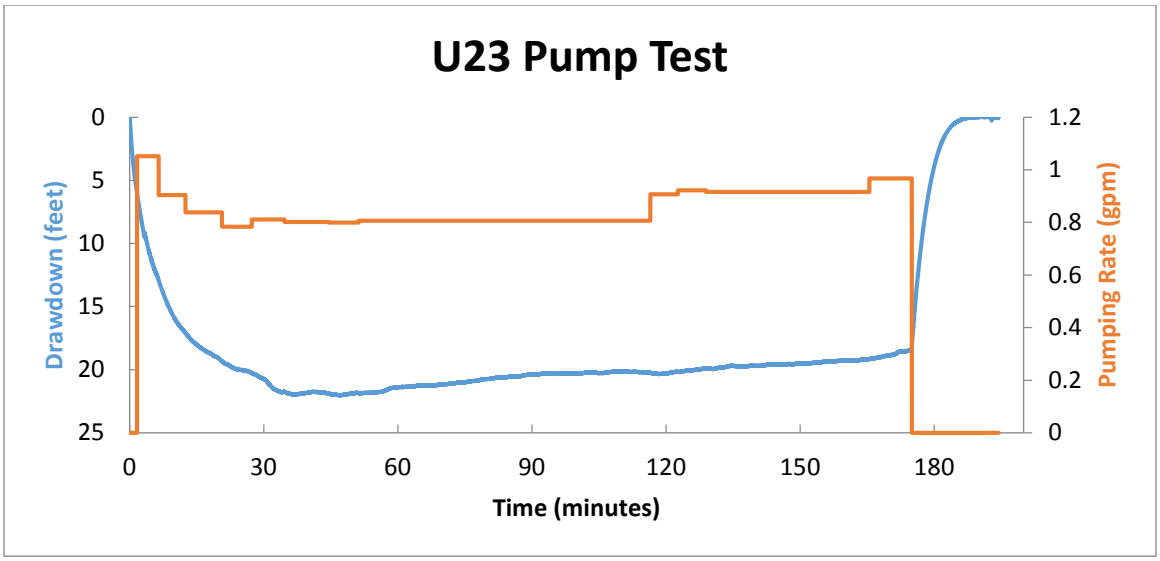
U23 Pump Test
Drawdown (feet)
0
5
10
15
20
25
Pumping Rate (gpm)
1.2
1
0.8
0.6
0.4
0.2
0
0
30
60
90
120
150
180
Time (minutes)

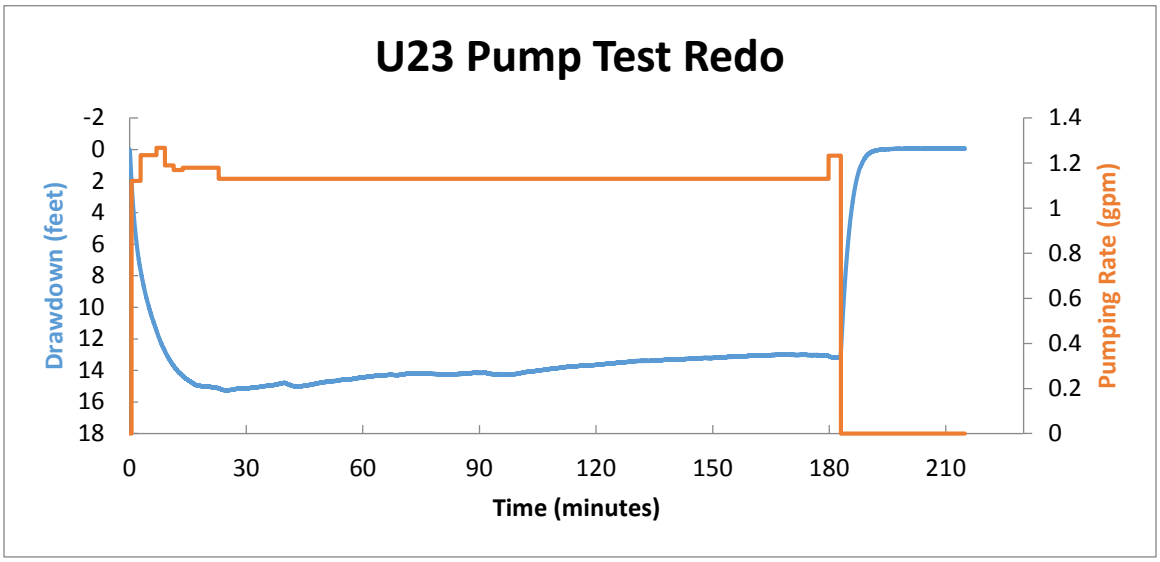
U23 Pump Test Redo
Drawdown (feet)
-2
0
2
4
6
8
10
12
14
16
18
Pumping Rate (gpm)
1.4
1.2
1
0.8
0.6
0.4
0.2
0
0
30
60
90
120
150
180
210
Time (minutes)

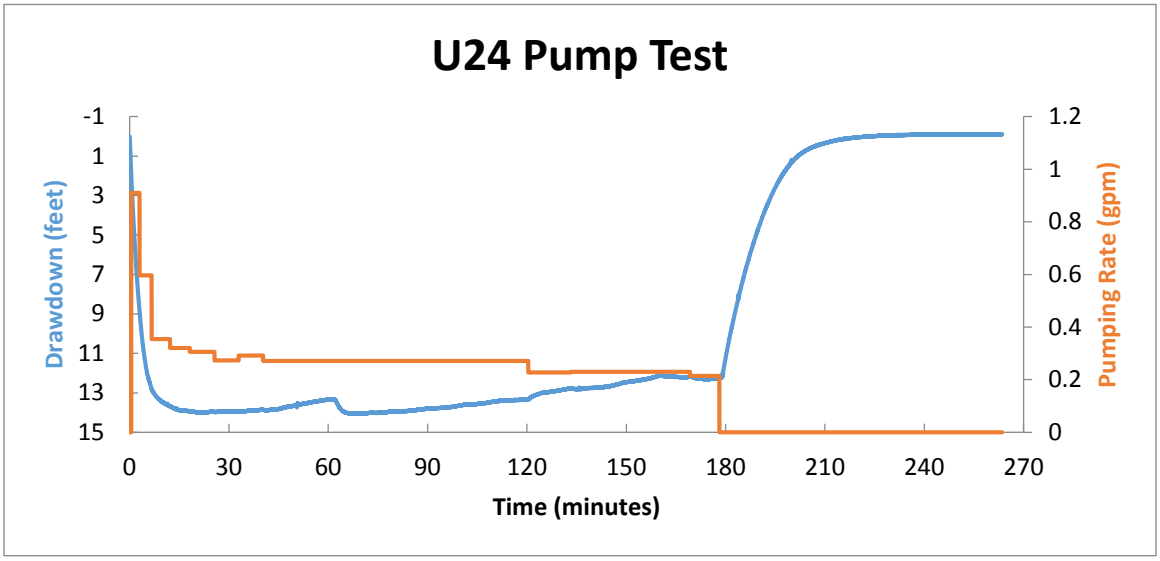
U24 Pump Test
Drawdown (feet)
-1
1
3
5
7
9
11
13
15
Pumping Rate (gpm)
1.2
1
0.8
0.6
0.4
0.2
0
0
30
60
90
120
150
180
210
240
270
Time (minutes)

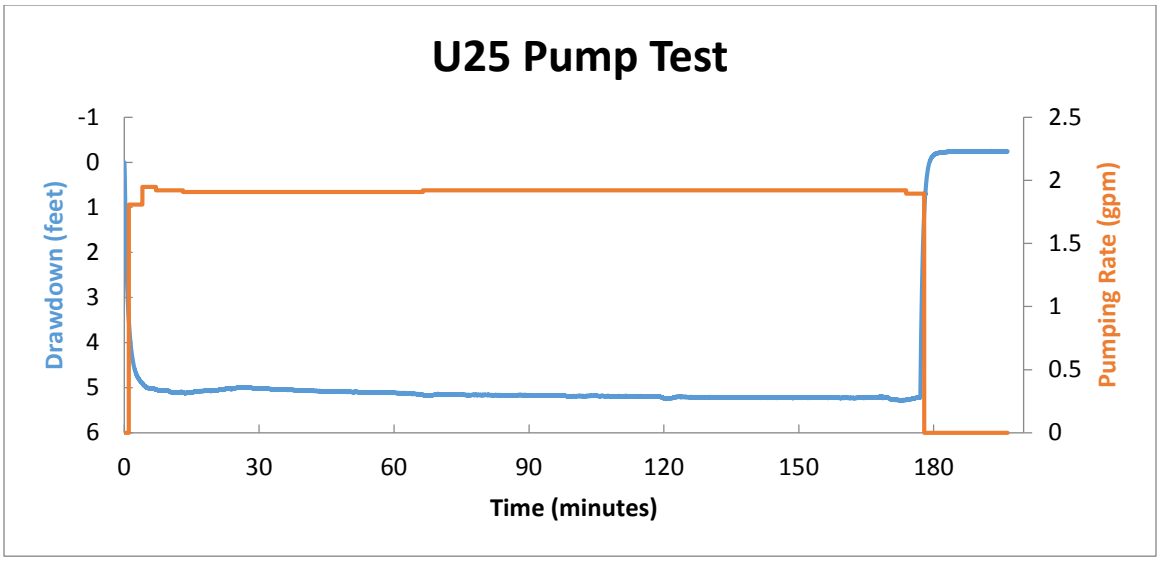
U25 Pump Test
Drawdown (feet)
-1
0
1
2
3
4
5
6
Pumping Rate (gpm)
2.5
2
1.5
1
0.5
0
0
30
60
90
120
150
180
Time (minutes)

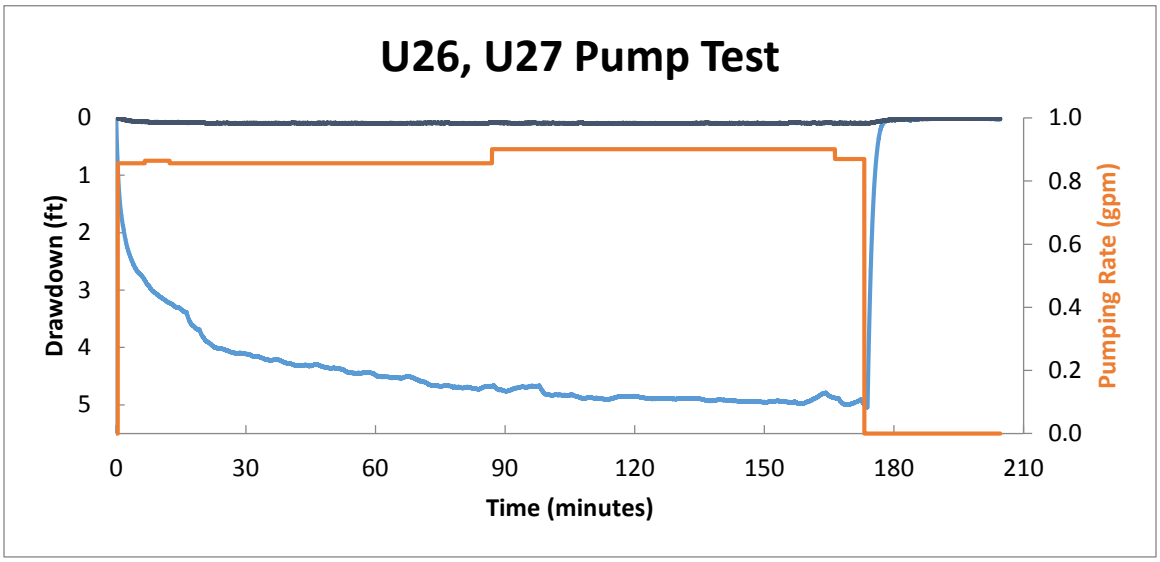
U26, U27 Pump Test
Drawdown (ft)
0
1
2
3
4
5
Pumping Rate (gpm)
1.0
0.8
0.6
0.4
0.2
0.0
0
30
60
90
120
150
180
210
Time (minutes)

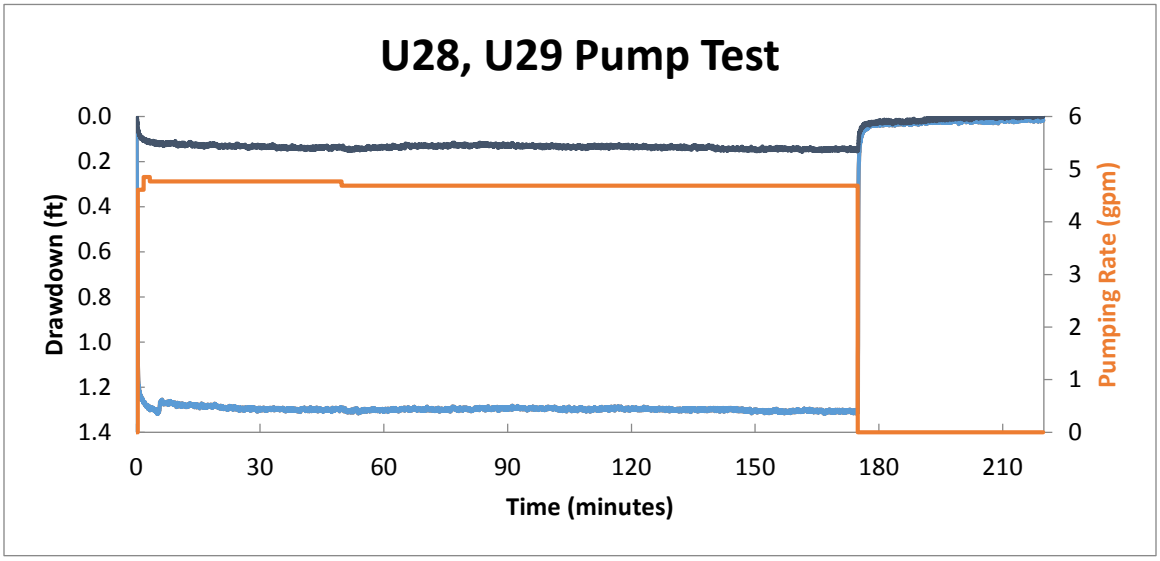
U28, U29 Pump Test
Drawdown (ft)
0.0
0.2
0.4
0.6
0.8
1.0
1.2
1.4
Pumping Rate (gpm)
6
5
4
3
2
1
0
0
30
60
90
120
150
180
210
Time (minutes)

REFERENCES

Aeschbach-Hertig, W., F. Peeters, U. Beyerle, and R. Kipfer, 1999, Interpretation of dissolved atmospheric noble gases in natural waters: Water Resources Research, v. 35, p. 2779-2792.

Aeschbach-Hertig, W., F. Peeters, U. Beyerle, and R. Kipfer, 2000, Palaeotemperature reconstruction from noble gases in ground water taking into account equilibration with entrapped air: Nature, v. 405, p. 1040-1044.

Brown, R., J. Ferris, C. Jacob, D. Knowles, R. Meyer, H. Skibitzke, and C. Theis, 1963, Methods of determining permeability, transmissibility and drawdown: US Geological Survey Water-Supply Paper, v. 1536, p. 341.

Bullister, J. L., D. P. Wisegarver, and F. A. Menzia, 2002, The solubility of sulfur hexafluoride in water and seawater: Deep Sea Research Part I: Oceanographic Research Papers, v. 49, p. 175-187.

Busenberg, E., and L. N. Plummer, 2000, Dating young groundwater with sulfur hexafluoride: Natural and anthropogenic sources of sulfur hexafluoride: Water Resources Research, v. 36, p. 3011-3030.

Clarke, W. B., W. Jenkins, and Z. Top, 1976, Determination of tritium by mass spectrometric measurement of 3He: The international journal of applied radiation and isotopes, v. 27, p. 515-522.

Cooper, H. H., and C. E. Jacob, 1946, A generalized graphical method for evaluating formation constants and summarizing well-field history: Eos, Transactions American Geophysical Union, v. 27, p. 526-534.

Craig, H., 1961, Isotopic variations in meteoric waters: Science, v. 133, p. 1702-1703.

Doelling, H. H., 1983, Observations on Paradox Basin salt anticlines, *in* Averett, W.R., editor, Northern Paradox Basin-Umconpaghre uplift: Grand Junction Geological Society Field Trip, p. 81-90.

Doelling, H. H., M. L. Ross, and W. E. Mulvey, 2002, Geologic map of the Moab 7.5'quadrangle, Grand County, Utah, Utah Geological Survey, Utah Department of Natural Resources.

Driscoll, F. G., 1986, Groundwater and wells: St. Paul, Minnesota: Johnson Filtration Systems Inc., 1986, 2nd ed., v. 1.

Fillmore, R., 2010, Geological Evolution of the Colorado Plateau of Eastern Utah and Western Colorado, Including the San Juan River, Natural Bridges, Canyonlands, Arches, and the Book Cliffs, University of Utah Press.

Gardner, P. M., 2004, Environmental Tracer Investigation of Groundwater Conditions at the Scott M. Matheson Wetlands Preserve Near Moab, Utah, University of Utah.

Halford, K. J., W. D. Weight, and R. P. Schreiber, 2006, Interpretation of transmissivity estimates from single-well pumping aquifer tests: Ground Water, v. 44, p. 467-471.

Heilweil, V. M., D. S. Sweetkind, and S. J. Gerner, 2014, Innovative environmental tracer techniques for evaluating sources of spring discharge from a carbonate aquifer bisected by a river: Groundwater, v. 52, p. 71-83.

Kaufman, S., and W. Libby, 1954, The natural distribution of tritium: Physical Review, v. 93, p. 1337.

Koh, D.-C., L. N. Plummer, E. Busenberg, and Y. Kim, 2007, Evidence for terrigenic SF 6 in groundwater from basaltic aquifers, Jeju Island, Korea: Implications for groundwater dating: Journal of Hydrology, v. 339, p. 93-104.

Lovelock, J. E., 1971, Atmospheric fluorine compounds as indicators of air movements: Nature, v. 230, p. 379.

Maiss, M., and I. Levin, 1994, Global increase of SF6 observed in the atmosphere: Geophysical Research Letters, v. 21, p. 569-572.

Manning, A. H., and D. K. Solomon, 2003, Using noble gases to investigate mountain-front recharge: Journal of Hydrology, v. 275, p. 194-207.

Pataki, D. E., S. Bush, P. Gardner, D. K. Solomon, and J. R. Ehleringer, 2005, Ecohydrology in a Colorado River riparian forest: implications for the decline of Populus fremontii: Ecological Applications, v. 15, p. 1009-1018.

Plummer, L. N., and E. Busenberg, 2000, Chlorofluorocarbons, Environmental tracers in subsurface hydrology, Springer, p. 441-478.

Solomon, D. K., and P. G. Cook, 2000, 3h and 3he, Environmental tracers in subsurface hydrology, Springer, p. 397-424.

Stute, M., and P. Schlosser, 2000, Atmospheric noble gases, Environmental tracers in subsurface hydrology, Springer, p. 349-377.

Sumsion, C., 1971, Geology and water resources of the Spanish Valley area: Grand and San Juan Counties, Utah: Utah Department of Natural Resources Technical Publication, v. 32, p. 45.

Theis, C. V., 1935, The relation between the lowering of the Piezometric surface and the rate and duration of discharge of a well using ground-water storage: Eos, Transactions American Geophysical Union, v. 16, p. 519-524.

Wilson, R. D., and D. M. Mackay, 1993, The use of sulphur hexafluoride as a conservative tracer in saturated sandy media: Ground Water, v. 31, p. 719-724.

http://www.noblegaslab.utah.edu/pdfs/cu_tube_sampling.pdf